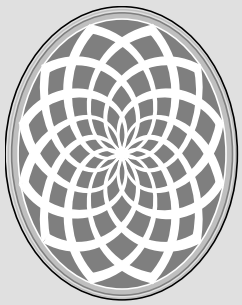

Interdisciplinary Mathematics Institute

2011:04

Kinetic Theories for Biofilms

Qi Wang and Tianyu Zhang

IMI

Preprint Series

College of Arts and Sciences
University of South Carolina

Kinetic Theories for Biofilms

Qi Wang *and Tianyu Zhang †

Abstract

We apply the kinetic theory formulation for binary complex fluids to develop a set of hydrodynamic models for the two-phase mixture of biofilms and solvent (water). It is aimed to model nonlinear growth and transport of the biomass in the mixture and the biomass-flow interaction. In the kinetic theory formulation of binary complex fluids, the biomass consisting of EPS (Extracellular Polymeric Substance) polymer networks and bacteria is coarse-grained into an effective fluid component, termed the effective polymer solution; while the other component, termed the effective solvent, is made up of the collective ensemble of nutrient substrates and the solvent. The mixture is modeled as an incompressible two-phase fluid in which the presence of the effective components are quantified by their respective volume fractions. The kinetic theory framework allows the incorporation of microscopic details of the biomass and its interaction with the coexisting effective solvent. The relative motion of the biomass and the solvent relative to an average velocity is described by binary mixing kinetics along with the intrinsic molecular elasticity of the EPS network strand modeled as an elastic dumbbell. This theory is valid in both the biofilm region which consists of the mixture of the biomass and solvent and the pure solvent region, making it convenient in numerical simulation of the biomass-flow interaction. Steady states and their stability are discussed under a growth condition. Nonlinear solutions of the three models developed in this study in simple shear are calculated and compared numerically.

1 Introduction

Biofilms, consisting of myriad microbes, their excretions, and trapped particles, are ubiquitous in nature, medical implants, rusty pipes, and dentistry etc., where microbes survive on wet surfaces. In principle, a biofilm community can be formed by a single bacterial species in damp environment; but, in nature, biofilms almost always consist of rich mixtures of multiple species of bacteria as well as fungi, algae, yeasts, protozoa, other microorganisms, debris and corrosion products etc. Biofilms are held together by a network of sugary molecular strands produced by the microbes, collectively termed "extracellular polymeric substances" or "EPS". In bacterial biofilms, bacterial cells are held together by the network consisting of the EPS strands produced by the bacteria, allowing them to develop complex, three-dimensional, resilient, attached communities [10, 11, 13, 28].

The center for disease control and national institute of health estimated that 65% to 85% of all chronic infections can be attributed to bacterial biofilms [11]. In human diseases, biofilm infections are some of the most recalcitrant to treat. Even with rigorous antibiotic regimens, some biofilms, such as those within the thick airway mucus of cystic fibrosis (CF) patients, persist throughout the course of the disease process [18]. One noted that the gene expression of a single bacterial (planktonic) cell differs drastically from that of the biofilm colonies indicating environmentally induced genetic change to the bacterial cell. This is one of the reason why antibiotics that are effective to treat single bacterium may not be effective in the

*Department of Mathematics and NanoCenter at USC, University of South Carolina, Columbia, SC 29208; Nankai University, Tianjin, P. R. China. Email: qwang@math.sc.edu

†Department of Mathematical Sciences, Montana State University, Bozeman, MT, 59717-2400. Email: zhang@math.montana.edu

treatment of the bacteria encased in biofilms. Bacterial biofilms can also be utilized in bio-terrorism in which persistent 'bio-terrorist agent biofilms' with Francisella tularensis can grow on surfaces where environmental amoeba can phagocytose them, allowing for growth of fibrosis [18]. Biofilms cost the U.S. literally billions of dollars every year in energy losses, equipment damage, product contamination and medical infections. Understanding the mechanism for the dynamical growth, transport, detachment and break-down of biofilms is important for improving water treatment, medical treatment of diseases, protecting equipment or device from corrosion and contamination, and even preventing bio-terrorism. It can have a profound impact on environmental sciences, medicine, civil engineering, naval sciences, military applications and homeland security.

Modeling biofilms has been a challenge given their complex cellular structures and changing genetic dynamics in the presence of foreign agents [10, 13, 28]. Biofilms essentially behave like biogels in which small solvent and nutrient molecule can permeate the network formed by the bacterial and the EPS strands. A set of discrete or semi-discrete models associated with cellular automata have been used to study the various aspect of the biofilm phenomena in multidimensional settings [29, 30, 31, 32]. Recently, there have emerged a host of continuum models for biofilms treating them as mixtures of multiple idealized species [9, 21, 34, 1, 38, 39]. In these models, the mixture is either modeled as a multi-fluid mixture [9, 21, 34, 1] or a single fluid of multi-components/species [38, 39]. In the multifluid models [9, 21, 1], which one uses in the development of hydrodynamical models for hydrogels, the velocity for each individual component is introduced and the balance laws for the mass and momentum of each species are preserved. The technical difficulty working with these multi-fluid models is that the individual velocity fields of the species are used as primary field variables in these theories; however they are essentially immeasurable in experiments since hydrodynamic measurements are often limited to the mean or average quantities in multiphase fluids. Moreover, the inflow and outflow boundary conditions for the individual species are elusive when it comes to mathematically solving the governing system of equations without additional simplifications. The single fluid multi-species model however can overcome this technical difficulty by providing explicit relative velocities in terms of the excessive velocities generated by nonequilibrium thermodynamics (mixing dynamics) with respect to an average bulk velocity [38, 39] and have been successfully used in modeling biofilm expansion/growth, shedding or streaming, detachment of biofilm blobs from large colonies, and rippling phenomenon under shear [39]. In this single fluid multi-component fluid system, the inter-penetration of different species is carried out by their respect entropy and the mixing free energy. This molecular mechanism compensates the so-called friction forces due to the relative motions among the various species commonly seen in the multi-fluid theories near hydrodynamic equilibrium. By devising appropriate intermolecular potential for the multiphase fluid, we can tailor our models to account for the physics of mixing effectively.

The mathematical models for hydrodynamics of biofilms available so far are primarily coarse-grain models in which little cellular kinetics is incorporated. There are some common ingredients in the multiphase fluid models for biofilms (either multi-fluid or single fluid ones) [9, 1, 21, 34, 38], in which the nutrient substrate is passively treated as a part of the solvent and the volume of the bacteria is collectively treated a part of the effective polymer. The effective polymer adopted here is also collectively identified as the biomass in the literature. In this paper, we interchangeably use the name of effective polymer or biomass in order to make contact with the complex fluid models to be developed as well as the biological community where biomass is the more familiar term.

The volume fraction of the biomass ϕ_n and that of the solvent ϕ_s are two basic hydrodynamic variables along with the velocity of the biomass $\mathbf{v}_n$ and the velocity of the solvent $\mathbf{v}_s$ in multifluid models or the average velocity $\mathbf{v}$ in single fluid multicomponent models, the concentration of the nutrient substrate c, the concentration of the bacteria B, the pressure p, and the polymeric stress for the effective polymer. The volume fraction of the biomass and the effective solvent are assumed to obey reaction-transport equations

in these models,

$$\begin{aligned} &\frac{\partial \phi_n}{\partial t} + \nabla \cdot (\phi_n \mathbf{v}_n) = g_n, \\ &\frac{\partial \phi_s}{\partial t} + \nabla \cdot (\phi_s \mathbf{v}_s) = g_s, \end{aligned} \tag{1.1}$$

where g_n and g_s is the polymer production rate and the solvent consumption rate, respectively. The bacterial production as well as the substrate consumption equation are given as follows:

$$\begin{aligned} &\frac{\partial B}{\partial t} + \nabla \cdot (B\mathbf{v}_n) = g_b, \\ &\frac{\partial}{\partial t}(\phi_s c) + \nabla \cdot (c\mathbf{v}_s \phi_s - D_s \phi_s \nabla c) = -g_c, \end{aligned} \tag{1.2}$$

where g_b is the production rate for the bacteria, g_c is the consumption rate of the nutrient substrate in the solvent, D_s is the diffusion constant for the nutrient.

The binary theories for biofilms differ in the formulation of various velocities in conservation of mass and momentum equations and the constitutive relations for g_n and g_s. Some end up with a quasi-compressible constraint for an average velocity [9, 21, 1] while others retain the incompressible constraint on the average velocity field [38]. Besides these differences, the constitutive equation for the stress and reactive rates are essentially the same when both the effective solvent and the effective polymer are treated as viscous fluids which is perfectly valid in the growth time scale of the biofilm. In this case, the extra stress tensor and some of the growth as well as decay rates are given by the following constitutive laws.

$$\begin{aligned} &\tau_n = 2\eta_n \mathbf{D}_n,\ \tau_s = 2\eta_s \mathbf{D}_s, \\ &g_c = \phi_n A \tfrac{c}{K_0 + c},\ g_n = \mu \phi_n \tfrac{c}{K_c + c}, \end{aligned} \tag{1.3}$$

where $\eta_{n,s}$ are the viscosity of the effective polymer and the solvent, respectively, $\mathbf{D}_{n,s} = \frac{1}{2}[\nabla \mathbf{v}_{n,s} + \nabla \mathbf{v}_{n,s}^T]$ is the rate of strain tensor for the effective polymer and the solvent, respectively, A is the maximum consumption rate of the nutrient substrate, μ is the maximum production rate of the biomass, K_0 and K_c are two half-saturation constants. We note that the bacterial concentration decouples from the rest of the equations in the binary biofilm models. It can thus be ignored completely in the models when the focus is on the growth of the biomass or effective polymer.

In the phase field model we developed in [38], the ensemble of the bacteria is effectively modeled as the "viscous solvent" which blends with the EPS network to function effectively as a polymer solution. A distribution function for the polymer network strands can then be introduced to describe the concentration of the polymer network strand in the "viscous solvent" as well as the coarse-grain or meso-structure of the polymer network. This thus motivates us to seek a kinetic formulation of biofilm theories to describe the EPS network immersed in the viscous bacterial bath and thereby to guide the study of the biomass-flow interaction.

In this paper, we refine our single fluid multicomponent formulation of biofilm theories by developing a set of kinetic theory models for biofilm-solvent mixtures systematically [2]. This new formulation of the biofilm models provides a well-structured theoretical framework for expanding the theory to incorporate additional molecular information and biochemical details of the biofilm components into the model as one's understanding of biofilm dynamics progresses. In what follows, we treat the biomass-solvent mixture as incompressible with a divergence-free average (bulk) velocity field and then develop a kinetic theory for the effective polymer and solvent mixture taking into account the polymer conformational dynamics of the EPS strand, production of biomass at the microscopic level, and the biomass-solvent interaction. Within this framework, a variety of molecular models can be crafted to account for the polymer network strand

(dumbbell, FENE dumbbell, Rouse chain, etc.) and a spectrum of polymer and solvent interaction dynamics can be proposed (like mixing theory of Flory-Huggins, etc.). A simplified mechanical model, the dumbbell model, for the EPS network strand and a kinetic network theory along with the Flory-Huggins mixing dynamics is set up to illustrate the idea and demonstrate how consistent stress expressions for the effective polymer can be derived. The kinetic theories developed here are de-facto phase field models with the field variable naturally given by the effective polymer (or biomass) volume fraction $\phi_n(\mathbf{x},t)$ (the zeroth moment of the effective polymer distribution function), in which the biofilm-solvent interface is given by the zero-level surface of the phase variable: $\lim_{\delta\to 0+}\{\mathbf{x}|\phi_n(\mathbf{x},t)=\delta\}$ [35, 36]. The biofilm region is presented by the non-vanishing biomass volume fraction variable ϕ_n. In this formulation, we tacitly assume the EPS density is directly proportional to the bacterial density and thereby a single volume fraction can be employed to represent the biomass. This phase field model provides a low (computational) cost mathematical formulation of the complex interfacial problem.

The rest of the paper is organized as follows. First we develop a set of kinetic theories for biofilms by accounting for transport of polymer network strands and their conformational changes as well as nutrient substrates, and the response of the polymer network in flow in three plausible ways within the theoretical framework of network theories for one fluid multi-component mixtures. We then analyze the stability of steady states to identify the unstable modes in long wave regimes. Finally, we study the biofilm expansion/growth in one space dimension numerically and compare the predictions made with the three different kinetic theories.

2 Kinetic Theories for Biofilms

We model the biofilm as a fluid mixture of two effective components: the biomass as the effective polymer solution including both the viscoelastic EPS polymer network and the viscous bacterial "solution", and the effective solvent consisting of the solvent and the dissolved nutrient substrate. In this theory, we neglect the mass of the nutrient and instead only account for its reactive effect. The EPS polymer network is described by network strands connected at junction points. The dynamics of the network consist of the dynamics of the center of mass of the polymer strand and the dynamics for the center of mass. This description clearly cast a two-scale view on the nature of the polymer network dynamics. The dynamics for the center of mass of the polymer strand can be described at the macroscopic or the continuum level; whereas the dynamics of the polymer strand relative to the center of mass belongs to the mesoscale. Based on this, we develop a kinetic theory for the fluid mixture accounting for the microstructure conformation of the polymer network strand as well as the interaction between the effective components, in which we model the strand in the EPS network using an elastic dumbbell model and bacteria as viscous fluids. In this setting, the effective polymer is effectively treated as a polymeric solution, where the EPS polymer network is "immersed" in the "bacterial solution."

We denote the statistical weight of a polymer network strand with its center of mass located at $\mathbf{x}$ and the end-to-end vector $\mathbf{q}$ at time t as $\psi(\mathbf{x},\mathbf{q},t)$ such that the polymer network volume fraction ϕ_n is defined as the zeroth moment of the statistical weight ψ with respect to the configuration variable $\mathbf{q}$,

$$\phi_n(\mathbf{x},t)=\int_{\mathbf{R}^3}\psi d\mathbf{q}=\langle 1\rangle, \tag{2.1}$$

where

$$\langle(\bullet)\rangle=\int_{\mathbf{R}^3}(\bullet)\psi d\mathbf{q}. \tag{2.2}$$

Notice that wherever the region is filled with pure solvent, i.e., $\phi_n(\mathbf{x},t)=0$, $\psi(\mathbf{x},\mathbf{q},t)=0$. Wherever $\phi_n(\mathbf{x},t)\neq 0$, however, a probability density function $\frac{\psi(\mathbf{x},\mathbf{q},t)}{\phi_n(\mathbf{x},t)}$ can be identified and a probability ensemble

average with respect to the conformation variable $\mathbf{q}$ can be defined by

$$\langle(\bullet)\rangle_q = \frac{1}{\phi_n(\mathbf{x},t)}\langle(\bullet)\rangle. \tag{2.3}$$

To make a distinction between the two ensemble averages defined above, we remark that $\langle\rangle_q$ is a probability ensemble average while $\langle\rangle$ is an ensemble proportional to the volume fraction ϕ. Apparently, the effective polymer volume fraction $\phi_n(\mathbf{x},t)$ plays the role of a phase field variable in the theory. I.e., when $\phi_n(\mathbf{x},t) = 0$, the fluid consists of entirely the solvent; otherwise, it is a true binary mixture. Therefore, the resulting theory serves as an effective phase field model. The two distinctive phases are differentiated by $\phi_n(\mathbf{x},t) = 0$ (solvent) and $\phi_n(\mathbf{x},t) > 0$ (biofilm mixture), respectively. For biofilms, $\phi_n(\mathbf{x},t) < 1$ is normally assumed, excluding the very unlikely situation where the biofilm is completely dry without any solvent.

In this model, we treat the entire material system as an incompressible single fluid mixture of two effective components, in which an average velocity $\mathbf{v}$ is assumed to exist and divergence free. We propose that the free energy density of the mixture system is composed of the mixing free energy for the solvent and the polymer network, elastic energy for the polymer network, self-energy of the polymer and the solvent respectively, and the conformational entropy for the polymer network strand (elastic dumbbell):

$$F = f_{int} + f_{ec} + f_{es} + f_{sol}, \tag{2.4}$$

where f_{int} is the extended Flory-Huggins mixing free energy density, f_{ec} is the entropic and the elastic energy density for the conformation of the polymer strand, f_{es} is the elastic energy for the polymer network, and f_{sol} is the self-energy for the solvent. Specifically,

$$f_{ec} = \nu k_B T \int_{\mathbf{R}^3} [\ln(\frac{\Psi}{\phi_n}) + \xi\|\mathbf{q}\|^2]\psi(\mathbf{x},\mathbf{q},t)d\mathbf{q}, \tag{2.5}$$

where $\xi\nu k_B T$ is the stiffness of the polymer chain, ν is the number density of the polymer chain and $(\ln\frac{\Psi}{\phi_n})\psi$ corresponds to the entropic contribution of the polymer chain, which is understood to be possibly nonzero only in the region where $\phi_n \neq 0$ and zero elsewhere; the extended Flory-Huggins mixing free energy density f_{int} as a function of ϕ_n is given by

$$f_{int} = k_B T \left[\frac{\gamma_1}{2}\|\nabla\phi_n\|^2 + \gamma_2\left(\frac{\phi_n}{N}\ln(\phi_n) + (1-\phi_n)\ln(1-\phi_n) + \chi\phi_n(1-\phi_n)\right)\right], \tag{2.6}$$

where γ_1 and γ_2 measures the strength of the entropic conformational and bulk mixing free energy, respectively, χ is the Flory-Huggin's mixing parameter, N is the generalized polymerization index for the polymer strand;

$$f_{es} = \phi_n f(\mathbf{B}), \tag{2.7}$$

where f_{es} is a prescribed function of the Finger tensor $\mathbf{B}$ whose transport equation is given by

$$\frac{\partial\mathbf{B}}{\partial t} + \nabla\cdot(\mathbf{v}_n\mathbf{B}) + \mathbf{W}_n\cdot\mathbf{B} - \mathbf{B}\cdot\mathbf{W}_n - a_1[\mathbf{D}_n\cdot\mathbf{B} + \mathbf{B}\cdot\mathbf{D}_n] + \frac{\mathbf{B}}{\lambda_2} = \frac{2\eta_b}{\lambda_2}\mathbf{D}_n = 2G_i\mathbf{D}_n, \tag{2.8}$$

where λ_2 is the relaxation time, $-1 \leq a_1 \leq 1$ is a model parameter, $\mathbf{v}_n$ is the network velocity (defined below), $\mathbf{W}_n$ and $\mathbf{D}_n$ are the vorticity and rate of deformation tensor associated to the network deformation, respectively, a_1 is a parameter between -1 and 1, η_b is a viscosity parameter and $G_i = \frac{\eta_b}{\lambda_2}$ is the elastic modulus;

$$f_{sol} = (1-\phi_n)C_{sol}, \tag{2.9}$$

where C_{sol} is the self-energy of the solvent which is a constant. Since f_{sol} is a linear function of the volume fraction, its contribution to the chemical potential is merely a constant and therefore can be neglected. We will thereby drop the self-energy of the solvent from the free energy functional to simplify the presentation. We note that $\gamma_2 = \nu N$ is proportional to the reciprocal of the volume of the solvent molecule and $\|\cdot\|$ denotes the l_2 norm of a vector. The entropic conformational free energy is included in the Flory-Huggins mixing free energy to minimize the spatial inhomogeneity in the biomass.

One choice of the nonlinear elastic energy for the deformation of the center of mass of the polymer strand in the network is given by

$$f(\mathbf{B}) = \xi_2 tr(\mathbf{B}) + \xi_3 \ln\det(\mathbf{B}), \tag{2.10}$$

where ξ_2 and ξ_3 are two model parameters. Then,

$$\frac{\partial f(\mathbf{B})}{\partial \mathbf{B}} = \xi_2 \mathbf{I} + \xi_3 \mathbf{B}^{-1}. \tag{2.11}$$

Given the free density functional, we can calculate the chemical potential of the polymer system as follows

$$\mu = \frac{\delta F}{\delta \psi} = \frac{\delta f_{int}}{\delta \psi} + \frac{\delta f_{ec}}{\delta \psi} + \frac{\delta f_{es}}{\delta \psi}, \tag{2.12}$$

where

$$\begin{aligned}
&\tfrac{\delta f_{ec}}{\delta \psi} = \nu\xi k_B T \|\mathbf{q}\|^2 + \nu k_B T [\ln \tfrac{\psi}{\phi_n}],\\
&\tfrac{\delta f_{int}}{\delta \psi} = \tfrac{\delta f_{int}}{\delta \phi_n} = -k_B T \gamma_1 \Delta\phi_n - \gamma_2 k_B T \left[\tfrac{-1}{N}(1+\ln(\phi_n)) + \ln(1-\phi_n) + 1 - \chi + 2\chi\phi_n\right],\\
&\tfrac{\delta f_{es}}{\delta \psi} = f(\mathbf{B}).
\end{aligned} \tag{2.13}$$

We note that the identity: $\frac{\delta \phi_n}{\delta \psi} = 1$ is used in the above derivation. So,

$$\mu = k_B T \left[\nu\xi\|\mathbf{q}\|^2 + \nu(\ln\frac{\psi}{\phi_n}) - \gamma_1\Delta\phi_n - \gamma_2[\frac{-1}{N}(\ln(\phi_n)) + \ln(1-\phi_n) + 2\chi\phi_n]\right] + f(\mathbf{B}) + const. \tag{2.14}$$

With the chemical potential, we next derive a set of kinetic models for the biofilm fluid. We will present three distinct versions by postulating three plausible ways that the conservative force in translational diffusion of the EPS network can be approximated in the mean-field.

2.1 Separable Model 1 for Biofilms

In the biomass, we assume (1). the creation rate and the annihilation rate of polymer network strands is balanced by a growth/production rate, (2). the translational diffusion is carried out through a configurational space averaged chemical potential, (3). the deformation of the EPS strand (elastic dumbbell) in the configurational space ($\mathbf{q}$) is due to the polymer velocity gradient $\nabla\mathbf{v}_n$ to be derived below. The transport equation for the statistical weight ψ is then given by the following Smoluchowski equation [3, 15]

$$\begin{aligned}
&\tfrac{\partial}{\partial t}\psi + \nabla\cdot(\mathbf{v}\psi) = \nabla\cdot(\lambda\nabla\langle\mu\rangle_q\psi) + \nabla_q\cdot\tfrac{1}{\zeta}(\nabla_q\mu\psi) - \nabla_q\cdot((\nabla\mathbf{v}_n + (a-1)\mathbf{D}_n)\cdot\mathbf{q}\psi) + G_n,\\
&G_n = \mu_r\tfrac{\psi c}{K_c + c},
\end{aligned} \tag{2.15}$$

where λ is the mobility coefficient, ζ is the friction coefficient for the rotational motion of the polymer chain, a is a slip parameter between -1 and 1 accounting for slippage between the polymer and the solvent, $\nabla \mathbf{v}_n$ is the velocity gradient tensor with respect to the polymer velocity, $\mathbf{D}_n = \frac{1}{2}[\nabla \mathbf{v}_n + \nabla \mathbf{v}_n^T]$ is the rate of strain tensor with respect to the polymer velocity, G_n is the polymer network strand production rate in unit volume in phase space $(\mathbf{x}, \mathbf{q})$, μ_r is the maximum growth rate of the biomass and K_c is a half-saturation constant for the nutrient consumption kinetics via a Michaelis-Menton model. We note that both λ and ζ can be second order tensors when the diffusion is anisotropic. In this paper, we adopt an isotropic diffusion coefficient tensor for illustration purposes though. To simplify the presentation, we stipulate that the ensemble average $\langle(\bullet)\rangle_q = 0$ whenever $\phi_n = 0$ throughout the paper.

2.1.1 Transport Equations For Volume Fractions And Structure Tensors: Low Order Moment Equations

Since polymer volume fraction ϕ_n is the zeroth moment of ψ, we obtain the transport equation of ϕ_n by integrating the Smoluchowski equation over the configurational space ($\mathbf{q}$-space),

$$\begin{aligned}
&\tfrac{\partial \phi_n}{\partial t} + \nabla \cdot (\phi_n \mathbf{v}) = \nabla \cdot [\lambda \phi_n \nabla \langle \mu \rangle_q] + g_n, \\
&g_n = \mu_r \tfrac{\phi_n c}{K_c + c}, \\
&\langle \mu \rangle_q = -k_B T \gamma_1 \Delta \phi_n - \gamma_2 k_B T \left[-\tfrac{\ln \phi_n}{N} + \ln(1-\phi_n) + 2\chi \phi_n \right] + \\
&\qquad \nu \xi k_B T \langle \|\mathbf{q}\|^2 \rangle_q + \nu k_B T \langle \ln(\tfrac{\psi}{\phi_n}) \rangle_q + f(\mathbf{B}) + const, \text{ in biofilm.}
\end{aligned} \tag{2.16}$$

We remark that the mobility vanishes in pure solvent and so does $\phi_n \langle \mu \rangle_q = 0$. So, this is a singular or modified Cahn-Hilliard equation [4, 5].

From the transport equation for the volume fraction, the local instantaneous velocity can be identified as consisting of two parts: the average velocity $\mathbf{v}$ and the excessive velocity due to the binary mixing. The latter contribution to the flux, which can be read off from the transport equation, is assumed proportional to the mixing force given by the gradient of the ensemble average of the chemical potential

$$\mathbf{v}_n^e = -\lambda \nabla \langle \mu \rangle_q. \tag{2.17}$$

It is called the excessive polymer velocity that is only defined in the biofilm region. The polymer velocity is then identified as

$$\mathbf{v}_n = \mathbf{v} + \mathbf{v}_n^e. \tag{2.18}$$

This polymer velocity is not a divergence-free vector although the average velocity $\mathbf{v}$ may be. In fact, this velocity coincides with the average velocity outside the biofilm region; so it is a globally defined hydrodynamic variable. Using this notation, the transport equation for ϕ_n simplifies to

$$\frac{\partial \phi_n}{\partial t} + \nabla \cdot (\phi_n \mathbf{v}_n) = g_n. \tag{2.19}$$

With this polymer velocity, we can define the rate of strain tensor and vorticity tensor associated with the velocity field:

$$\mathbf{D}_n = \frac{1}{2}(\nabla \mathbf{v}_n + \nabla \mathbf{v}_n^T), \mathbf{W}_n = \frac{1}{2}(\nabla \mathbf{v}_n - \nabla \mathbf{v}_n^T). \tag{2.20}$$

We now introduce the second moment of $\mathbf{q}$ with respect to ψ:

$$\mathbf{Q} = \langle \mathbf{qq} \rangle = \phi_n \langle \mathbf{qq} \rangle_q. \tag{2.21}$$

The transport equation for the second order tensor $\mathbf{Q}$ is obtained from the Smoluchowski equation (2.15) by multiplying it with $\mathbf{qq}$ and then integrating it over the configurational space ($\mathbf{q}$):

$$\frac{\partial}{\partial t}\mathbf{Q} + \nabla \cdot (\mathbf{v}_n \mathbf{Q}) - \mathbf{W}_n \cdot \mathbf{Q} + \mathbf{Q} \cdot \mathbf{W}_n - a[\mathbf{D}_n \cdot \mathbf{Q} + \mathbf{Q} \cdot \mathbf{D}_n] = \frac{2\nu k_B T}{\zeta}(\phi_n \mathbf{I} - 2\xi \mathbf{Q}) + \tilde{g}_n \mathbf{Q}, \tag{2.22}$$

where $\tilde{g}_n = \frac{\mu_r c}{k_c + c}$.

When $\phi_n \neq 0$, we introduce the second moment of $\mathbf{q}$ with respect to a probability density function

$$\mathbf{M} = \langle \mathbf{qq} \rangle_q, \;\; \mathbf{Q} = \phi_n \mathbf{M}. \tag{2.23}$$

The transport equation for $\mathbf{M}$ is given by

$$\phi_n \left[\frac{\partial}{\partial t}\mathbf{M} + \mathbf{v}_n \cdot \nabla \mathbf{M} - \mathbf{W}_n \cdot \mathbf{M} + \mathbf{M} \cdot \mathbf{W}_n - a[\mathbf{D}_n \cdot \mathbf{M} + \mathbf{M} \cdot \mathbf{D}_n] \right] = \frac{2\nu \phi_n k_B T}{\zeta}(\mathbf{I} - 2\xi \mathbf{M}). \tag{2.24}$$

Canceling $\phi_n \neq 0$, we arrive at

$$\frac{\partial}{\partial t}\mathbf{M} + \mathbf{v}_n \cdot \nabla \mathbf{M} - \mathbf{W}_n \cdot \mathbf{M} + \mathbf{M} \cdot \mathbf{W}_n - a[\mathbf{D}_n \cdot \mathbf{M} + \mathbf{M} \cdot \mathbf{D}_n] = \frac{2\nu k_B T}{\zeta}(\mathbf{I} - 2\xi \mathbf{M}). \tag{2.25}$$

We emphasize that this equation is valid only if $\phi_n \neq 0$. For simulation purposes, the quantity $\mathbf{Q}$ is well defined globally and easier to handle since it vanishes in the pure solvent region along with $\phi_n = 0$.

We next assume the statistical weight ψ is separable, i.e., it is a product of the pdf ψ_n in the configurational space of the dumbbell chains and the volume fraction ϕ_n:

$$\psi(\mathbf{x}, \mathbf{q}, t) = \phi_n(\mathbf{x}, t)\psi_n(\mathbf{x}, \mathbf{q}, t). \tag{2.26}$$

Then, the average chemical potential reduces to

$$\langle \mu \rangle_q = -k_B T \gamma_1 \Delta \phi_n - \gamma_2 k_B T \left[-\tfrac{\ln \phi_n}{N} + \ln(1 - \phi_n) + 2\chi \phi_n \right] + \nu \xi k_B T \langle \|\mathbf{q}\|^2 \rangle_q + \nu k_B T \langle \ln \psi_n \rangle_q + f(\mathbf{B}). \tag{2.27}$$

Combining the Smoluchowski equation and equation (2.19), we arrive at the equation for the configurational pdf ψ_n at $\phi_n \neq 0$

$$\frac{d}{dt}\psi_n = \frac{\partial}{\partial t}\psi_n + \mathbf{v}_n \cdot \nabla(\psi_n) = \nabla_q \cdot \frac{1}{\zeta} \nabla_q \mu \psi_n - \nabla_q \cdot ((\nabla \mathbf{v}_n + (a-1)\mathbf{D}_n) \cdot \mathbf{q}\psi_n). \tag{2.28}$$

It can be readily verified that the second moment equation of the pdf ψ_n is given exactly by (2.25).

Notice that the incompressibility condition $\phi_s + \phi_n = 1$ requires

$$\frac{\partial \phi_s}{\partial t} + \nabla \cdot (\phi_s \mathbf{v}) = -\lambda \nabla \cdot (\phi_n \nabla \langle \mu \rangle_q) - g_n. \tag{2.29}$$

From this transport equation for ϕ_s, the excessive solvent velocity can be identified as

$$\mathbf{v}_s^e = \lambda \frac{\phi_n}{\phi_s} \nabla \langle \mu \rangle_q. \tag{2.30}$$

The actual solvent velocity is calculated by

$$\mathbf{v}_s = \mathbf{v} + \mathbf{v}_s^e. \tag{2.31}$$

Then, we arrive at that the average velocity $\mathbf{v}$ is in fact the volume averaged velocity

$$\mathbf{v} = \phi_n \mathbf{v}_n + \phi_s \mathbf{v}_s. \tag{2.32}$$

Hence, the transport equation for ϕ_s can be recast into

$$\frac{\partial \phi_s}{\partial t} + \nabla \cdot (\phi_s \mathbf{v}_s) = -g_n. \tag{2.33}$$

The nutrient substrate is assumed to be transported along with the solvent velocity. Its transport equation is given by

$$\frac{\partial}{\partial t}(\phi_s c) + \nabla \cdot (c\mathbf{v}_s\phi_s - D_s\phi_s\nabla c) = -g_c, \tag{2.34}$$

where c is the nutrient concentration per unit volume of solvent, $\phi_s c$ is the actual concentration per unit biofilm volume, and $g_c = A\phi_n \frac{c}{K_0+c}$ is the consumption rate for the nutrient. Here A is a maximum constant decay rate and k_o is the half-saturation constant in this model.

When the solvent is modeled as a viscous fluid, the constitutive equation for the extra stress in solvent is given by

$$\tau_s = 2\eta_s \mathbf{D}_s, \tag{2.35}$$

where η_s is the solvent viscosity and $\mathbf{D}_s = \frac{1}{2}[\nabla \mathbf{v}_s + \nabla \mathbf{v}_s^T]$ is the rate of strain tensor with respect to the solvent velocity.

Given the transport equations for the volume fractions, the elastic deformation tensor $\mathbf{B}$, and the second order tensor $\mathbf{Q}$, we next derive the elastic stress tensor to couple the meso-structural variables $(\phi_n, \mathbf{Q})$ and the continuum variable $\mathbf{B}$ to the macroscopic momentum transport of the fluid mixture.

2.1.2 Constitutive Stress Equations For Effective Polymers

The extra stress for the polymer in the mixture will supply the crucial link to close the governing system of equations for the biofilm model. Given the composition of the biomass, its contribution to the stress tensor consists of two parts: the viscous stress $\phi_n \tau_{ps}$ due to the viscous bacteria and the elastic stress due to the EPS network. The bacterial viscous stress is given by

$$\tau_{ps} = 2\eta_{ps} \mathbf{D}_n, \tag{2.36}$$

where η_p is the bacterial viscosity. We use a virtual work principle to calculate the elastic stress of the polymer. We define the free energy of the mixture system as

$$A = \int F d\mathbf{x}, \tag{2.37}$$

where the free energy density F is given by (2.4). The variation of the free energy density is calculated as follows

$$\delta F = \frac{\delta(f_{int} + f_{es})}{\delta \phi_n}\delta\phi_n + \frac{\delta f_{ec}}{\delta \psi}\delta\psi + \frac{\delta f_{es}}{\delta \mathbf{B}} : \delta\mathbf{B}. \tag{2.38}$$

We use

$$\begin{aligned}
&\delta\phi_n = \tfrac{\partial}{\partial t}\phi_n\delta t = -\nabla\cdot(\mathbf{v}_n\phi_n)\delta t,\\
&\delta\psi = \tfrac{\partial}{\partial t}\psi\delta t = -\nabla\cdot(\mathbf{v}_n\psi)\delta t - \nabla_q\cdot((\nabla\mathbf{v}_n + (a-1)\mathbf{D}_n)\cdot\mathbf{q}\psi)\,\delta t,\\
&\delta\mathbf{B} = \tfrac{\partial\mathbf{B}}{\partial t}\delta t = [-[\nabla\cdot(\mathbf{v}_n\mathbf{B}) + \mathbf{W}_n\cdot\mathbf{B} - \mathbf{B}\cdot\mathbf{W}_n - a_1[\mathbf{D}_n\cdot\mathbf{B} + \mathbf{B}\cdot\mathbf{D}_n]] + 2G_i\mathbf{D}_n]\delta t,
\end{aligned} \tag{2.39}$$

assuming that the virtual time scale δt is so small that the virtual deformation dominates the other motions. It then follows that

$$\begin{aligned}
&\delta A = \int \tfrac{\delta f_{int}+\delta f_{es}}{\delta\phi_n}(-\nabla\cdot(\mathbf{v}_n\phi_n))\delta t d\mathbf{x} - \int\int \tfrac{\delta f_{ec}}{\delta\psi}[\nabla\cdot(\mathbf{v}_n\psi) + \nabla_q\cdot((\nabla\mathbf{v}_n + (a-1)\mathbf{D}_n)\cdot\mathbf{q}\psi)]\delta t d\mathbf{x} d\mathbf{q} -\\
&\int \tfrac{\delta f_{es}}{\delta B} : [[\nabla\cdot(\mathbf{v}_n\mathbf{B}) + \mathbf{W}_n\cdot\mathbf{B} - \mathbf{B}\cdot\mathbf{W}_n - a_1[\mathbf{D}_n\cdot\mathbf{B} + \mathbf{B}\cdot\mathbf{D}_n]] - 2G_i\mathbf{D}_n]\delta t d\mathbf{x}.
\end{aligned} \tag{2.40}$$

From the above expression, we identify the elastic force as

$$\mathbf{F}_e = -\phi_n\nabla(\tfrac{\delta f_{int}}{\delta\phi_n} + \tfrac{\delta f_{es}}{\delta\phi_n}) - \langle\nabla\tfrac{\delta f_{ec}}{\delta\psi}\rangle - (\nabla\tfrac{\delta f_{es}}{\delta B}) : \mathbf{B} = -\gamma_1 k_B T\nabla\cdot(\nabla\phi_n\nabla\phi_n) - \phi_n\nabla f(\mathbf{B}) - \nabla p_1 - \nabla\tfrac{\delta f_{es}}{\delta B_{ij}}B_{ij}, \tag{2.41}$$

where p_1 is a scalar functional of ϕ_n, and the elastic stress as

$$\begin{aligned}
&\tau_e = \tfrac{(a+1)}{2}\langle\nabla_q\tfrac{\delta f_{ec}}{\delta\psi}\mathbf{q}\rangle + \tfrac{(a-1)}{2}\langle\mathbf{q}\nabla_q\tfrac{\delta f_{ec}}{\delta\psi}\rangle + \tfrac{(a_1+1)}{2}\tfrac{\delta f_{es}}{\delta\mathbf{B}}\cdot\mathbf{B} + \tfrac{(a_1-1)}{2}\mathbf{B}\cdot\tfrac{\delta f_{es}}{\delta\mathbf{B}} +\\
&G_i(\tfrac{\delta f_{es}}{\delta\mathbf{B}} + (\tfrac{\delta f_{es}}{\delta\mathbf{B}})^T).
\end{aligned} \tag{2.42}$$

Combining $\mathbf{F}^e$ and τ_e, the extra elastic stress tensor for the effective polymer is expressed as

$$\tau_n^e = -\gamma_1 k_B T\nabla\phi_n\nabla\phi_n + 2a\xi\nu k_B T\phi_n\mathbf{M} + a_1\tfrac{\delta f_{es}}{\delta\mathbf{B}}\cdot\mathbf{B} + G_i(\tfrac{\delta f_{es}}{\delta\mathbf{B}} + (\tfrac{\delta f_{es}}{\delta\mathbf{B}})^T). \tag{2.43}$$

Here we assume f_{es} is made up of all bulk terms. If we introduce

$$\tau = 2\xi\nu k_B T(\mathbf{M} - \frac{\mathbf{I}}{2\xi}), \tag{2.44}$$

then, τ satisfies the following transport equation,

$$\frac{\partial\tau}{\partial t} + \mathbf{v}_n\cdot\nabla\tau - \mathbf{W}_n\cdot\tau + \tau\cdot\mathbf{W}_n - a[\mathbf{D}_n\cdot\tau + \tau\cdot\mathbf{D}_n] + \frac{\tau}{\lambda_1} = \frac{2\eta_n}{\lambda_1}\mathbf{D}_n. \tag{2.45}$$

where $\lambda_1 = \frac{\zeta}{4\xi\nu k_B T}$ is the relaxation time, $\eta_n = \frac{a\zeta}{4\xi}$ is the EPS polymer viscosity [3]. The rubber-elastic model can be viewed as a limiting case of the current model as $\lambda_1 \to \infty$ and $a = 1$. Since $2a\xi\nu k_B T\phi_n\mathbf{M} = a\phi_n\tau + a\nu k_B T\phi_n\mathbf{I}$, by absorbing $a\nu k_B T\phi_n\mathbf{I}$ into the pressure term, the total extra stress is given by

$$\begin{aligned}
&\tau_{total} = \phi_s\tau_s + \phi_n\tau_{ps} + \tau_n^e = \phi_s\tau_s - \gamma_1 k_B T\nabla\phi_n\nabla\phi_n + a\phi_n\tau + \phi_n\tau_{ps} + a_1\tfrac{\delta f_{es}}{\delta\mathbf{B}}\cdot\mathbf{B} +\\
&G_i(\tfrac{\delta f_{es}}{\delta\mathbf{B}} + (\tfrac{\delta f_{es}}{\delta\mathbf{B}})^T).
\end{aligned} \tag{2.46}$$

After combining the terms that can be identified as a part of the stress, the elastic force is left with

$$\mathbf{F}_e = -\phi_n\nabla f(\mathbf{B}) - \nabla\frac{\delta f_{es}(\mathbf{B})}{\delta\mathbf{B}} : \mathbf{B} - \nabla p_1. \tag{2.47}$$

In summary, the kinetic theory for biofilms consists of four sets of equations.

Momentum and continuity equation

$$\begin{aligned}
&\nabla\cdot\mathbf{v}=0,\\
&\rho\tfrac{d\mathbf{v}}{dt}=\nabla\cdot(a\phi_n\tau+\phi_n\tau_{ps}+\phi_s\tau_s+a_1\tfrac{\delta f_{es}}{\delta\mathbf{B}}\cdot\mathbf{B}+G_i(\tfrac{\delta f_{es}}{\delta\mathbf{B}}+(\tfrac{\delta f_{es}}{\delta\mathbf{B}})^T))\\
&-\left[\nabla p+\gamma_1 k_BT\nabla\cdot(\nabla\phi_n\nabla\phi_n)+\phi_n\nabla f(\mathbf{B})+\nabla\tfrac{\delta f_{es}}{\delta\mathbf{B}}:\mathbf{B}\right].
\end{aligned}\tag{2.48}$$

Here the velocity is approximated as solenoidal and the hydrodynamic pressure p contains various scalar functionals of ϕ_n and $\mathbf{B}$ as well as the static pressure.

Transport equation for the nutrient

$$\tfrac{\partial}{\partial t}(\phi_s c)+\nabla\cdot(c\mathbf{v}_s\phi_s-D_s\phi_s\nabla c)=-g_c.\tag{2.49}$$

Transport equation for the effective polymer volume fraction

$$\tfrac{\partial\phi_n}{\partial t}+\nabla\cdot(\phi_n\mathbf{v})=\nabla\cdot[\lambda\phi_n\nabla\langle\mu\rangle_q]+g_n.\tag{2.50}$$

Constitutive equations for stress tensors

$$\begin{aligned}
&\tfrac{\partial\tau}{\partial t}+\mathbf{v}_n\cdot\nabla\tau-\mathbf{W}_n\cdot\tau+\tau\cdot\mathbf{W}_n-a[\mathbf{D}_n\cdot\tau+\tau\cdot\mathbf{D}_n]+\tfrac{\tau}{\lambda_1}=\tfrac{2\eta_n}{\lambda_1}\mathbf{D}_n,\tau_{ps}=2\eta_p\mathbf{D}_n,\tau_s=2\eta_s\mathbf{D}_s,\\
&\tfrac{\partial\mathbf{B}}{\partial t}+\nabla\cdot(\mathbf{v}_n\mathbf{B})+\mathbf{W}_n\cdot\mathbf{B}-\mathbf{B}\cdot\mathbf{W}_n-a_1[\mathbf{D}_n\cdot\mathbf{B}+\mathbf{B}\cdot\mathbf{D}_n]+\tfrac{\mathbf{B}}{\lambda_2}=2G_i\mathbf{D}_n.
\end{aligned}\tag{2.51}$$

2.2 Separable Model 2 for Biofilms

Instead of using the ensemble averaged chemical potential to calculate the force in the spatial transport of ψ, we adopt an averaged force $\langle\nabla\mu\rangle_q$. The Smoluchowski equation for ψ is modified to

$$\tfrac{\partial}{\partial t}\psi+\nabla\cdot(\mathbf{v}\psi)=\nabla\cdot(\lambda\langle\nabla\mu\rangle_q\psi)+\nabla_q\cdot\tfrac{1}{\zeta}(\nabla_q\mu\psi)-\nabla_q((\nabla\mathbf{v}_n+(a-1)\mathbf{D}_n)\cdot\mathbf{q}\psi)+G_n.\tag{2.52}$$

The zero moment of the pdf is

$$\begin{aligned}
&\tfrac{\partial\phi_n}{\partial t}+\nabla\cdot(\phi_n\mathbf{v})=\nabla\cdot[\lambda\langle\nabla\mu\rangle_q\phi_n]+g_n,\\
&\langle\nabla\mu\rangle_q=\nabla[-k_BT\gamma_1\Delta\phi_n-\gamma_2k_BT\left[-\tfrac{\ln\phi_n}{N}+\ln(1-\phi_n)+2\chi\phi_n\right]+f(\mathbf{B})]=\nabla\tfrac{\delta\hat{F}}{\delta\phi_n},
\end{aligned}\tag{2.53}$$

where $\hat{F}=f_{int}+f_{es}$. Note that the effective polymer velocity is given by

$$\mathbf{v}_n=\mathbf{v}-\lambda\nabla\frac{\delta\hat{F}}{\delta\phi_n},\tag{2.54}$$

while the solvent velocity is

$$\mathbf{v}_s=\mathbf{v}+\lambda\frac{\phi_n}{(1-\phi_n)}\nabla\frac{\delta\hat{F}}{\delta\phi_n}.\tag{2.55}$$

By taking the second moment of $\mathbf{q}$ with respect to the pdf ψ, we arrive at equation (2.22). The extra stress tensor in this model is identical to the one derived in the previous section. The difference lies in the definition of the polymer velocity $\mathbf{v}_n$ though.

If we set $\psi=\phi_n\psi_n$, the transport equation for ψ_n is given exactly by (2.28). This version of the model without the network center of mass (the Finger tensor) elasticity was studied in details in [38, 39], where it was introduced phenomenologically. Now, we have shown that the model can be cast into a low moment projection of a kinetic model.

2.3 Nonseparable Model for Biofilms

The above two models are developed using the separability of the statistical weight ψ under two slightly different mean-field assumptions in the spatial or translational transport. We next consider the third model. Instead of the ensemble averaged chemical potential or averaged force, we use the same chemical potential in both the translational and configurational space transport in the Smoluchowski equation for the transport of ψ,

$$\frac{\partial}{\partial t}\psi + \nabla\cdot(\mathbf{v}\psi) = \nabla\cdot(\lambda\nabla\mu\psi) + \nabla_q\cdot\frac{1}{\zeta}(\nabla_q\mu\psi) - \nabla_q((\nabla\mathbf{v}_n + (a-1)\mathbf{D}_n)\cdot\mathbf{q}\psi) + G_n. \tag{2.56}$$

The zero moment of the pdf with respect to the configuration variable $\mathbf{q}$ is

$$\begin{aligned}
&\frac{\partial\phi_n}{\partial t} + \nabla\cdot(\phi_n\mathbf{v}) = \nabla\cdot[\lambda\langle\nabla\mu\rangle] + g_n,\\
&\langle\nabla\mu\rangle = \phi_n\langle\nabla\mu\rangle_q = \phi_n\nabla[-k_BT\gamma_1\Delta\phi_n -\\
&\gamma_2 k_BT\left[-\frac{\ln\phi_n}{N} + \ln(1-\phi_n) + 2\chi\phi_n\right] + f(\mathbf{B})] = \phi_n\nabla\frac{\delta\hat{F}}{\delta\phi_n}.
\end{aligned} \tag{2.57}$$

Notice that this transport equation is identical to the one derived using Model 2. We take the second moment of $\mathbf{q}$ with respect to ψ,

$$\begin{aligned}
&\frac{\partial}{\partial t}\mathbf{Q} + \nabla\cdot(\mathbf{v}_n\mathbf{Q}) - \mathbf{W}_n\cdot\mathbf{Q} + \mathbf{Q}\cdot\mathbf{W}_n - a[\mathbf{D}_n\cdot\mathbf{Q} + \mathbf{Q}\cdot\mathbf{D}_n]\\
&= \nabla\cdot(\lambda\langle(\nabla\mu - \langle\nabla\mu\rangle_q)\mathbf{q}\mathbf{q}\rangle) + \frac{2\nu k_BT}{\zeta}(\phi_n\mathbf{I} - 2\xi\mathbf{Q}) + \tilde{g}_n\mathbf{Q}\\
&= \nabla\cdot(\lambda\langle\nabla\frac{\delta f_{ec}}{\delta\psi}\mathbf{q}\mathbf{q}\rangle) + \frac{2\nu k_BT}{\zeta}(\phi_n\mathbf{I} - 2\xi\mathbf{Q}) + \tilde{g}_n\mathbf{Q}\\
&= \nabla\cdot[\lambda\nu k_BT(\nabla\mathbf{Q} - \nabla\ln\phi_n\mathbf{Q})] + \frac{2\nu k_BT}{\zeta}(\phi_n\mathbf{I} - 2\xi\mathbf{Q}) + \tilde{g}_n\mathbf{Q}.
\end{aligned} \tag{2.58}$$

Using $\mathbf{Q} = \phi_n\mathbf{M}$, it follows that

$$\begin{aligned}
&\phi_n\left[\frac{\partial}{\partial t}\mathbf{M} + \mathbf{v}_n\cdot\nabla\mathbf{M} - \mathbf{W}_n\cdot\mathbf{M} + \mathbf{M}\cdot\mathbf{W}_n - a[\mathbf{D}_n\cdot\mathbf{M} + \mathbf{M}\cdot\mathbf{D}_n]\right] =\\
&\phi_n\left[\frac{1}{\phi_n}\nabla\cdot[\lambda\phi_n\nu k_BT\nabla\mathbf{M}] + \frac{2\nu k_BT}{\zeta}(\mathbf{I} - 2\xi\mathbf{M})\right].
\end{aligned} \tag{2.59}$$

When $\phi_n \neq 0$, it yields

$$\frac{\partial}{\partial t}\mathbf{M} + \mathbf{v}_n\cdot\nabla\mathbf{M} - \mathbf{W}_n\cdot\mathbf{M} + \mathbf{M}\cdot\mathbf{W}_n - a[\mathbf{D}_n\cdot\mathbf{M} + \mathbf{M}\cdot\mathbf{D}_n] = \frac{1}{\phi_n}\nabla\cdot[\lambda\nu\phi_n k_BT\nabla\mathbf{M}] + \frac{2\nu k_BT}{\zeta}(\mathbf{I} - 2\xi\mathbf{M}). \tag{2.60}$$

In this model, the pdf ψ is not assumed separable. Thus, we call it a nonseparable model. The elastic stress constitutive equations is dissipative and all stress constitutive equations are given by

$$\frac{d\tau}{dt} - \mathbf{W}_n\cdot\tau + \tau\cdot\mathbf{W}_n - a[\mathbf{D}_n\cdot\tau + \tau\cdot\mathbf{D}_n] + \frac{\tau}{\lambda_1} = \frac{2\eta_n}{\lambda_1}\mathbf{D}_n + \frac{\lambda_3}{\lambda_1\phi_n}\nabla\cdot(\phi_n\nabla\tau), \tau_{ps} = 2\eta_p\mathbf{D}_n, \quad \tau_s = 2\eta_s\mathbf{D}_s \tag{2.61}$$

where $\lambda_3 = \frac{\lambda\zeta}{4\xi} = \frac{\lambda\eta_n}{a}$ is a parameter characterizing the stress diffusive length scale. $\frac{\lambda_3}{\lambda_1}$ defines the stress diffusion coefficient. In practice, especially, in numerical simulation, we use $\tau_n = \phi_n\tau$. It's zero when $\phi_n = 0$. The transport equation deduced from those of τ and ϕ_n.

$$\frac{\partial\tau_n}{\partial t} + \nabla\cdot(\mathbf{v}_n\tau_n) - \mathbf{W}_n\cdot\tau_n + \tau_n\cdot\mathbf{W}_n - a[\mathbf{D}_n\cdot\tau_n + \tau_n\cdot\mathbf{D}_n] + \frac{\tau_n - 2\eta_n\phi_n\mathbf{D}_n}{\lambda_1} = \frac{\lambda_3}{\lambda_1}\nabla\cdot(\nabla\tau_n - \nabla ln\phi_n\tau_n) + \tilde{g}_n\tau_n \tag{2.62}$$

Here *Bi* is a elastic modulus. (This needs to be checked.)

3 Closure Approximation to Separable Model 1 and Remarks

In Separable Model 1 for biofilms, the transport equation for ϕ_n is given by (2.16). This model couples the Smoluchowski equation for ψ_n to the transport of the volume fraction ϕ_n. In order to decouple them, we employ an approximation to the averaged chemical potential term $\langle \ln \psi_n \rangle_q$. We assume the equilibrium pdf of the polymer strand obeys the Gaussian distribution when the creation and annihilation rate cancels each other:

$$\psi_n = \frac{1}{\sqrt{2\pi}^3 \sqrt{\det \mathbf{M}}} e^{-\frac{1}{2}\mathbf{M}^{-1}:\mathbf{qq}}. \tag{3.1}$$

We replace the pdf ψ_n by this equilibrium pdf in $\langle \ln \psi_n \rangle_q = \int \ln \psi_n \psi_n d\mathbf{q}$ to yield:

$$\int \ln \psi_n \psi_n d\mathbf{q} = -\frac{1}{2} \ln(\det \mathbf{M}) + const. \tag{3.2}$$

Then,

$$\begin{aligned} \nabla \langle \mu \rangle_q = \nabla \left[-k_B T \gamma_1 \Delta \phi_n - \gamma_2 k_B T \left[-\tfrac{1}{N} - \tfrac{\ln \phi_n}{N} + \ln(1-\phi_n) + 1 - \chi + 2\chi\phi_n \right] + f(\mathbf{B}) \right] + \\ \nu k_B T \nabla \left(\xi \operatorname{tr} \mathbf{M} - \tfrac{1}{2} \ln(\det \mathbf{M}) \right). \end{aligned} \tag{3.3}$$

With this closure approximation, the transport equation for ϕ_n only couples to the transport equation for the second moment tensor $\mathbf{Q}$ or the elastic stress τ_n. Consequently, the Smoluchowski equation is successfully decoupled from the governing system of equations for the mixture.

Remark 1: Reformulation of Stress Constitutive Equations

Analogous to (2.62), we can compute elastic stress tensor $\tau_n = \phi_n \tau$ everywhere in the mixture through its transport equation derived from the second moment equation in the models directly. In separable model 1 and 2, it is given by

$$\frac{\partial \tau_n}{\partial t} + \nabla \cdot (\mathbf{v}_n \tau_n) - \mathbf{W}_n \cdot \tau_n + \tau_n \cdot \mathbf{W}_n - a[\mathbf{D}_n \cdot \tau_n + \tau_n \cdot \mathbf{D}_n] + \frac{\tau_n}{\lambda_1} = \frac{2\eta_n \phi_n}{\lambda_1} \mathbf{D}_n + \tilde{g}_n \tau_n. \tag{3.4}$$

The cost of computing this set of equations is comparable to that for the stress tensor τ. For comparison purposes with the results in [38], we will focus our analysis and numerical results on the set of variables $\phi_n, \tau, \mathbf{v}$ and their transport equations in this paper.

Remark 2: Model extension

In the aforementioned derivation, the polymer network strand is modeled using the simplest molecular model, the elastic dumbbell or bead-spring model. More realistic models such as various FENE models, network models and other polymer models can be incorporated effortlessly. If further information on the polymer network properties such as its strand creation and breakage rate aside from the polymer production due to bacteria is known a priori, the polymer network dynamics can be described in more details. When any nonlinear molecular model is incorporated into the configurational and translational dynamics, the resulting theory is most likely nonlinear so that the Smoluchowski equation is strongly coupled to the momentum transport equations. Therefore, the cost of solving the solutions of the system can pose a new challenge if a decoupled stress constitutive equation is not attainable.

Next, we compare the predictions made by the three biofilm models in one space dimension. *Given the similarity in the viscoelastic equation for the center of mass dynamics of the polymer strand and that of the polymer strand itself, we neglect the viscoelastic dynamics for the center of mass in the rest of the paper. This is equivalent to using one elastic relaxation time constitutive equation for the biomass.*

4 Nondimensionalization and Boundary Conditions

We use a characteristic time scale t_0, length scale h, and the nutrient concentration scale c_0 to nondimensionalize the variables

$$\tilde{t} = \frac{t}{t_0}, \tilde{\mathbf{x}} = \frac{\mathbf{x}}{h}, \tilde{\mathbf{q}} = \frac{\mathbf{q}}{h}, \tilde{\mathbf{v}} = \frac{\mathbf{v}t_0}{h}, \tilde{p} = \frac{ph^2}{f_0}, \tilde{\tau} = \frac{\tau h^2}{f_0}, \tilde{c} = \frac{c}{c_0}, \tag{4.1}$$

where f_0 is a characteristic force scale. The following dimensionless parameters arise

$$\begin{aligned} &\Lambda = \tfrac{\lambda t_0 f_0}{h^4},\ \Gamma_1 = \tfrac{\gamma_1 k_B T}{f_0},\ \Gamma_2 = \tfrac{\gamma_2 k_B T h^2}{f_0},\ Re_s = \tfrac{f_0 t_0}{\eta_s h^2},\ Re_n = \tfrac{f_0 t_0}{\eta_n h^2}, Re_{ps} = \tfrac{f_0 t_0}{\eta_{ps} h^2},\ \tilde{D}_s = \tfrac{D_s t_0}{h^2}, \\ &Bi = \tfrac{\rho_0 h^4}{f_0 t_0^2}, \tilde{\rho} = B_i(\phi_s \tfrac{\rho_s}{\rho_0} + \phi_n \tfrac{\rho_n}{\rho_0}),\ \tilde{A} = A t_0,\ \tilde{\mu}_r = \mu_r t_0,\ \tilde{K}_c = \tfrac{K_c}{c_0},\ \tilde{K}_0 = \tfrac{K_0}{c_0},\ \Lambda_1 = \tfrac{\lambda_1}{t_0},\ \Lambda_3 = \tfrac{\lambda \eta_n}{h^2 a}. \end{aligned} \tag{4.2}$$

where $\tilde{\rho}_0$ is an averaged density, $Bi = 1$ is set to define the characteristic force scale $f_0 = \frac{\rho_0 h^4}{t_0^2}$ as the inertia force. We summarize the description of the dimensionless parameters below:

- Re_s, Re_{ps} and Re_n are the Reynolds number for the solvent, bacterial "solvent" and EPS polymer, respectively.
- Λ is the dimensionless mobility.
- Γ_1 and Γ_2 measure the strength of the conformational entropy and the bulk mixing free energy.
- Bi is a parameter for the inertia, which is set to be 1 in this study.
- $\tilde{D}_s$ is the dimensionless diffusion coefficient for the nutrient.
- $\tilde{\mu}_r$ is the dimensionless biomass maximum growth rate and $\tilde{A}$ is the dimensionless decay rate for the nutrient.
- $\tilde{K}_c, \tilde{K}_0$ are the dimensionless half saturation constants.
- Λ_1 is the Deborah number for the EPS polymer.
- $\tilde{\rho}$ is the dimensionless density of the mixture.
- $\Lambda_3 = \frac{\Lambda}{aRe_n}$ is the effective stress diffusion constant.

For simplicity, we drop the ˜ on the dimensionless variables and the parameters. The system of governing equations of separable model 2 in these dimensionless variables is listed below

$$\begin{aligned} &\nabla \cdot \mathbf{v} = 0, \\ &\rho \tfrac{d\mathbf{v}}{dt} = \nabla \cdot (\phi_n (a\tau + \tfrac{2}{Re_{ps}} \mathbf{D}_n) + \phi_s \tfrac{2}{Re_s} \mathbf{D}_s) - [\nabla p + \Gamma_1 \nabla \cdot (\nabla \phi_n \nabla \phi_n)], \\ &\tfrac{\partial}{\partial t}(\phi_s c) + \nabla \cdot (c \mathbf{v}_s \phi_s - D_s \phi_s \nabla c) = -g_c, \\ &\tfrac{\partial \phi_n}{\partial t} + \nabla \cdot (\phi_n \mathbf{v}) = \nabla \cdot [\Lambda \phi_n \nabla \tfrac{\delta \hat{F}}{\delta \phi_n}] + g_n, \\ &\Lambda_1 \left[\tfrac{\partial}{\partial t} \tau + \mathbf{v}_n \cdot \nabla(\tau) - \mathbf{W}_n \cdot \tau + \tau \cdot \mathbf{W}_n - a[\mathbf{D}_n \cdot \tau + \tau \cdot \mathbf{D}_n] \right] + \tau = \tfrac{2}{Re_n} \mathbf{D}_n, \end{aligned} \tag{4.3}$$

where

$$g_c = A\phi_n \frac{c}{K_0+c},\ g_n = \mu_r \phi_n \frac{c}{K_c+c},\ \mathbf{v}_n = \mathbf{v} - \Lambda \nabla \frac{\delta \hat{F}}{\delta \phi_n},\ \mathbf{v}_s = \mathbf{v} + \frac{\Lambda \phi_n}{\phi_s} \nabla \frac{\delta \hat{F}}{\delta \phi_n}.$$

The dimensionless mixing free energy density is now given by

$$f = \frac{\Gamma_1}{2} \|\nabla \phi_n\|^2 + \Gamma_2 \left[\frac{\phi_n}{N} \ln \phi_n + (1-\phi_n) \ln(1-\phi_n) + \chi \phi_n (1-\phi_n) \right], \tag{4.4}$$

Analogously, the other dimensionless equations can be obtained. To save space, we will only enumerate the ones that differ from the corresponding equations in separable model 2 listed above. For separable model 1, the governing system of equations consists of all equations in (4.3) except that the transport equation for ϕ_n is replaced by the following:

$$\begin{aligned} &\tfrac{\partial \phi_n}{\partial t} + \nabla \cdot (\phi_n \mathbf{v}) = \nabla \cdot [\Lambda \phi_n \nabla \langle \mu \rangle_q] + g_n, \\ &\nabla \langle \mu \rangle_q = \nabla \left[-\Gamma_1 \Delta \phi_n - \Gamma_2 \left[-\tfrac{\ln \phi_n}{N} + \ln(1-\phi_n) + 2\chi \phi_n \right] \right] + \tfrac{1}{2} \nabla (\mathrm{tr}(\tau) - \tfrac{\Gamma_2}{N} \ln \det(\tau + \tfrac{\Gamma_2}{N} \mathbf{I})). \end{aligned} \tag{4.5}$$

The governing system of equations in the nonseparable model is given by (4.3) except that the constitutive elastic stress equation is replaced by by

$$\Lambda_1 \left[\tfrac{\partial}{\partial t} \tau + \mathbf{v}_n \cdot \nabla(\tau) - \mathbf{W}_n \cdot \tau + \tau \cdot \mathbf{W}_n - a[\mathbf{D}_n \cdot \tau + \tau \cdot \mathbf{D}_n] \right] + \tau = \tfrac{2}{Re_n} \mathbf{D}_n + \tfrac{\Lambda_3}{\phi_n} \nabla \cdot (\phi_n \nabla \tau). \tag{4.6}$$

The boundary conditions for the moments are derived from the boundary condition for the statistical weight ψ in the Smoluchowski equation in each model. For the three models, they are respectively,

$$\begin{aligned} &\mathbf{n} \cdot \nabla \langle \mu \rangle_q \psi = 0, \text{ (Separable Model 1)}, \\ &\mathbf{n} \cdot \langle \nabla \mu \rangle_q \psi = 0, \text{ (Separable Model 2)}, \\ &\mathbf{n} \cdot \nabla \mu \psi = 0, \text{ (Nonseparable Model)}. \end{aligned} \tag{4.7}$$

where $\mathbf{n}$ is the unit external normal of the boundary. Taking the zero moment of the above equations, we arrive at the boundary condition for ϕ_n in the models, respectively. For the volume fraction ϕ_n, an additional flux condition has to be imposed in all three models:

$$\mathbf{n} \cdot \nabla \phi_n = 0. \tag{4.8}$$

The boundary conditions for the volume fraction ϕ_n in the nonseparable model are:

$$\mathbf{n} \cdot \nabla \phi_n = 0, \quad \mathbf{n} \cdot \langle \nabla \mu \rangle = 0. \tag{4.9}$$

The second boundary condition in the above translates into

$$\phi_n \mathbf{n} \cdot \nabla \frac{\delta \hat{F}}{\delta \phi_n} = 0. \tag{4.10}$$

Combining with the first boundary condition on ϕ_n, we arrive at

$$\phi_n \mathbf{n} \cdot \nabla [\Gamma_1 \nabla^2 \phi_n] = 0. \tag{4.11}$$

We take the liberty to set

$$\mathbf{n}\cdot\nabla^3\phi_n = 0. \tag{4.12}$$

Taking the second moment over eq. (4.7-c), we arrive at the boundary condition for the second moment tensor:

$$\mathbf{n}\cdot\langle\nabla\mu\mathbf{q}\mathbf{q}\rangle = 0. \tag{4.13}$$

This can be rewritten into the boundary condition in the elastic stress tensor τ:

$$\phi_n\mathbf{n}\cdot\left[\frac{\Gamma_2}{N}\nabla\tau+\nabla\frac{\delta\hat{F}}{\delta\phi_n}(\tau+\frac{\Gamma_2}{N}\mathbf{I})\right] = 0. \tag{4.14}$$

It translates into

$$\phi_n\mathbf{n}\cdot\nabla\tau = 0. \tag{4.15}$$

Once again, we make the choice to set

$$\mathbf{n}\cdot\nabla\tau = 0. \tag{4.16}$$

The boundary condition for the nutrient is the flux-free boundary condition at the solid wall ($\mathbf{n}\cdot\nabla c = 0$) and the Dirichlet boundary condition ($c = c^*$) at any boundaries that have access to a nutrient reservoir.

The boundary conditions in separable model 2 are identical except that there are no boundary conditions for the stress tensor τ since the stress constitutive equation in this model is no longer diffusive. The boundary conditions for separable model 1 are similar to those of model 2 except that the second condition for ϕ_n is now given by

$$\mathbf{n}\cdot\nabla\langle\mu\rangle_q = \mathbf{n}\cdot\left[\nabla\left[-\Gamma_1\Delta\phi_n\right]+\frac{1}{2}\nabla(\mathrm{tr}(\tau)-\frac{\Gamma_2}{N}\ln\det(\tau+\frac{\Gamma_2}{N}\mathbf{I}))\right] = 0. \tag{4.17}$$

5 Steady States in 1-D and Their Linear Stability

In this section we examine the solution of the governing system of equations that depend on one space variable $y \in I = [0,1]$. For the models under the zero elastic stress and zero nutrient concentration condition, the three models share the same set of nontrivial steady states governed by the singular steady state Cahn-Hilliard equation subject to the normal flux free boundary condition. The set of steady states is given by

$$\phi_n = \phi_0,\ c = 0,\ \tau = 0,\ \mathbf{v} = \mathbf{0}. \tag{5.1}$$

We linearized the equations about the constant states and then apply the normal mode analysis. In the linearized systems, the normal modes of elastic stress components decouple from those of ϕ_n and velocity $\mathbf{v}$. The decay rate in separable model 1 and 2 are identical and given by

$$-\frac{1}{\Lambda_1}, \tag{5.2}$$

while in the nonseparable model given by,

$$-\frac{1}{\Lambda_1}(1+\Lambda_3 k^2), \tag{5.3}$$

where k is the wave number of the infinitesimal perturbation. The growth rate for ϕ_n is identical in all three models given by

$$-\Lambda\phi_0 k^2(\Gamma_1 k^2 + \Gamma_2 \hat{f}''(\phi_0)), \tag{5.4}$$

where $\hat{f} = -[\frac{\phi_n}{N}\ln\phi_n + (1-\phi_n)\ln(1-\phi_n) + \chi\phi_n(1-\phi_n)]$ is the bulk mixing free energy density. The modes for the velocity and pressure are all decay, which can be found in [38]. If $\hat{f}''(\phi_0)$ is negative, a long-wave instability emerges for $0 \le |k| \le \sqrt{-\frac{\Gamma_2\hat{f}''(\phi_0)}{\Gamma_1}}$.

Another steady state solution family is given by

$$\phi_n = 0,\ c = c_0,\ \tau = 0,\ \mathbf{v} = \mathbf{0}, \tag{5.5}$$

where c_0 is a constant. The linearized stability analysis for this set of solution shows a growth given by g_n in all models in all wave numbers. The corresponding growth rate is given by

$$\frac{\mu_r c_0}{k_c + c_0} \tag{5.6}$$

These two "growth" mechanisms dictate the biomass dynamics in the near equilibrium state and also impact the nonlinear dynamics. The detail about the derivation of the linearized growth rate for the separable model 2 can be found in [38].

One of the characteristics of the biofilm is its time-dependent dynamical growth. In the rest of the paper, we will focus on the comparison of transient solutions of the nonlinear govern systems in the three models.

6 Numerical Scheme for Transient Biofilm Models in One Space Dimension

In this section we discuss the numerical methods used for solving the nonlinear systems of partial differential equations with emphasis on dynamical growth and transport of the biomass that is homogeneous in (x,z), namely, the 1-D biofilms with space variable $y \in I = [0,1]$. All unknowns are function of (y,t) only. We denote $\mathbf{v} = (v_x, v_y, v_z)$, $\mathbf{v}_n^e = (0, v_y^e, 0)$. Then, continuity equation along with the boundary conditions implies $v_y = 0$. So, $\mathbf{v}_n = \mathbf{v} + \mathbf{v}_n^e = (v_{nx}, v_{ny}, v_{nz}) = (v_x, v_y^e, v_z)$. Consequently, $\mathbf{v}_s = \mathbf{v} + \mathbf{v}_s^e = (v_{sx}, v_{sy}, v_{sz}) = (v_x, v_{sy}^e, v_z)$. Using the boundary condition and the momentum balance equation, we arrive at

$$p = -\Gamma_1(\phi_{n,y})^2 + 2\left(\frac{1-\phi_n}{Re_s}\frac{\partial v_{sy}}{\partial y} + \frac{\phi_n}{Re_{ps}}\frac{\partial v_{ny}}{\partial y}\right) + (a\phi_n\tau_{yy}). \tag{6.1}$$

We recall that separable model 1 differs from separable model 2 in that its excessive flux for the ϕ_n transport equation has an extra term $\frac{1}{2}\Lambda\phi_n\nabla\left(\mathrm{tr}(\tau) - \frac{\Gamma_2}{N}\ln\det\left(\tau + \frac{\Gamma_2}{N}\mathbf{I}\right)\right)$. Likewise, the nonseparable model differs from separable model 2 in the transport equation for the extra elastic stress which has an extra diffusive term $\frac{\Lambda_2}{\phi_n}\nabla\cdot(\phi_n\nabla\tau)$ on the right hand side of the stress evolutionary equation in the nonseparable model.

In the comparative study, we impose the following boundary conditions for separable model 2:

$$\begin{aligned} &v_x|_{y=0} = 0,\ v_x|_{y=1} = v_{shear},\ v_y|_{\partial I} = 0,\\ &\nabla\phi_n\cdot\mathbf{n}|_{\partial I} = \left[\mathbf{v} - \Lambda\nabla\frac{\delta F}{\delta\phi_n}\right]\cdot\mathbf{n}|_{\partial I} = 0,\\ &[D\phi_s\nabla c]\cdot\mathbf{n}|_{y=0} = 0,\ c|_{y=1} = c^\star, \end{aligned} \tag{6.2}$$

where ∂I are the end points of interval I. For the nonseparable model, additional boundary conditions must be imposed for the stress tensor

$$\nabla\tau_{xy}\cdot\mathbf{n}|_{\partial I} = \nabla\tau_{yy}\cdot\mathbf{n}|_{\partial I} = 0, \cdots. \tag{6.3}$$

For separable model 1, one of the boundary conditions for the volume fraction ϕ_n ($\mathbf{n}\cdot\nabla^3\phi_n = 0$ is replaced by

$$\mathbf{n}\cdot\nabla\left[-\Gamma_1\nabla^2\phi_n + \frac{1}{2}(\mathrm{tr}(\tau) - \frac{\Gamma_2}{N}\ln\det(\tau + \frac{\Gamma_2}{N}\mathbf{I}))\right] = 0. \tag{6.4}$$

The numerical scheme used to study the nonlinear dynamics of biofilm growth is a finite difference scheme with uniform spatial and time step sizes, denoted by Δy and Δt, respectively. Assuming interval $I = [0,1]$ is divided into M uniform sub-intervals with size $\Delta y = 1/M$ at $M+1$ nodes $y_0, y_1, \cdots, y_M$, we denote the values of the numerical solution of $\phi_n, c, v_x, \tau_{xy}, \tau_{yy}$ at $(n\Delta t, j\Delta y)$ by $\phi^n_{n,j}, c^n_j, v^n_{x,j}, \tau^n_{xy,j}, \tau^n_{yy,j}$. Since $\mathbf{v}\cdot\mathbf{n}|_{\partial I} = 0$, the discrete form of the boundary conditions (6.2) and (6.3) yield

$$\begin{aligned}
&\phi^n_{n,1} = \phi^n_{n,-1},\ \phi^n_{n,2} = \phi^n_{n,-2},\ \phi^n_{n,M+1} = \phi^n_{n,M-1},\ \phi^n_{n,M+2} = \phi^n_{n,M-2},\ c^n_1 = c^n_{-1},\ c^n_M = c^\star,\\
&v^n_{x,0} = 0,\ v^n_{x,M} = v_{shear},\ \tau^n_{xy,1} = \tau^n_{xy,-1},\ \tau^n_{xy,M+1} = \tau^n_{xy,M-1},\ \tau^n_{yy,1} = \tau^n_{yy,-1},\ \tau^n_{yy,M+1} = \tau^n_{yy,M-1}.
\end{aligned} \tag{6.5}$$

For given solutions at time step $n-1$ and n, the polymer volume fraction at time step $n+1$, ϕ^{n+1}_n is calculated by a $\theta-$method ($0 \le \theta \le 1$):

$$\begin{aligned}
&\tfrac{1}{\Delta t}(\phi^{n+1}_n - \phi^n_n) + \theta\nabla\cdot\left[\mathbf{v}^{n+1}\phi^{n+1}_n + \Lambda\bar{\phi}^{n+1}_n\nabla\left(\Gamma_1\nabla^2\phi^{n+1}_n + 2\Gamma_2\chi\phi^{n+1}_n\right)\right]\\
= \quad & g_n(\bar{\phi}^{n+\theta}_n, \bar{c}^{n+\theta}) - (1-\theta)\nabla\cdot\left[\mathbf{v}^n\phi^n_n + \Lambda\phi^n_n\nabla\left(\Gamma_1\nabla^2\phi^n_n + 2\Gamma_2\chi\phi^n_n\right)\right] -\\
& \Lambda\Gamma_2\nabla\cdot\left[\left(-\tfrac{\nabla\phi^{n+\theta}_n}{N} + \phi^{n+\theta}_n\nabla\ln(1-\bar{\phi}^{n+\theta}_n)\right)\right].
\end{aligned} \tag{6.6}$$

After this, the volume fraction of the solvent at time step $n+1$ is obtained by $\phi^{n+1}_s = 1 - \phi^{n+1}_n$ and the substrate concentration at time step $n+1$, c^{n+1}, is calculated by

$$\begin{aligned}
&\tfrac{1}{\Delta t}\left(\phi^{n+1}_s c^{n+1} - \phi^n_s c^n\right) - \theta\nabla\cdot\left(D_s\phi^{n+1}_s\nabla c^{n+1} - \phi^{n+1}_s\mathbf{v}^{n+1}_s c^{n+1}\right)\\
= \quad & -g_c(\bar{\phi}^{n+\theta}_n, \bar{c}^{n+\theta}) + (1-\theta)\nabla\cdot\left(D_s\phi^n_s\nabla c^n - \phi^n_s\mathbf{v}^n_s c^n\right).
\end{aligned} \tag{6.7}$$

The spatial discretization in all semidiscretized equations is done using central differences to ensure the second order accurate in space and volume preserving for ϕ_n when the growth is turned off. Here, the extrapolation is accomplished by $\bar{\phi}^{n+\theta}_n = (1+\theta)\phi^n_n - \theta\phi^{n-1}_n$, $\bar{c}^{n+\theta} = (1+\theta)c^n - \theta c^{n-1}$ and the nonlinear functions g_n, g_c and some terms involving log-function are evaluated at these extrapolated values. We use $\theta = 1/2$ in our simulations, thus the overall scheme is second order in time and space.

The average velocity components v_x and the stress components $\tau_{xy}, \tau_{yy}, \cdots$ are computed as follows. The time discretization of the equation for v_x is given by

$$\rho^{n+1}\frac{v^{n+1}_x - v^n_x}{\Delta t} - \theta\frac{\partial}{\partial y}\left(\left(\frac{\phi^{n+1}_s}{Re_s} + \frac{\phi^{n+1}_n}{Re_{ps}}\right)\frac{\partial v^{n+1}_x}{\partial y}\right) = (1-\theta)\frac{\partial}{\partial y}\left(\left(\frac{\phi^n_s}{Re_s} + \frac{\phi^n_n}{Re_{ps}}\right)\frac{\partial v^n_x}{\partial y}\right) + \frac{\partial(a\phi^n_n\tau^n_{xy})}{\partial y}. \tag{6.8}$$

The spatial discretization is again central difference.

For separable model 1 and 2, all six components of the stress tensor satisfy a generic equation of the form

$$\frac{\partial\tau_{ij}}{\partial t} + v^e_y\frac{\partial\tau_{ij}}{\partial y} = F_{ij}(\tau, \nabla\mathbf{v}_n). \tag{6.9}$$

Here $F_{ij}(\tau, \mathbf{v})$ represents the (i,j) component of the stress tensor and it doesn't contain terms involving partial derivatives of τ. Since $v^e_y = 0$ at $y = 0, 1$, there are no boundary conditions for the elastic stress tensor

τ necessary; thus, τ actually satisfies an ODE $\frac{\partial \tau}{\partial t} = F(\tau, \mathbf{v})$ at $y = 0, 1$. Then at the discrete level, we solve τ_0, τ_M by the following Runge-Kutta method.

$$\tau^{n+1} = \tau^n + \frac{\Delta t}{6}(K_1 + 2K_2 + 2K_3 + K_4), \tag{6.10}$$

where

$$K_1 = F(\tau^n, \nabla \mathbf{v}_n^n), \qquad K_2 = F(\tau^n + \frac{\Delta t}{2}K_1, \nabla[\frac{\mathbf{v}_n^n + \mathbf{v}_n^{n+1}}{2}]),$$
$$K_3 = F(\tau^n + \frac{\Delta t}{2}K_2, \nabla[\frac{\mathbf{v}_n^n + \mathbf{v}_n^{n+1}}{2}]), \quad K_4 = F(\tau^n + \Delta t K_3, \nabla \mathbf{v}_n^{n+1}).$$

We solve $\tau_j^n, 1 \le j \le M-1$, by the following upwind scheme

$$\frac{\tau_j^{n+1} - \tau_j^n}{\Delta t} = -\frac{1}{2\Delta y}\Big\{[1 - \text{sign}(v_{y,j+1/2}^{e,n})]v_{y,j+1/2}^{e,n}(\tau_{j+1}^n - \tau_j^n) + [1 + \text{sign}(v_{y,j-1/2}^{e,n})]v_{y,j-1/2}^{e,n}(\tau_j^n - \tau_{j-1}^n)\Big\} + F(\tau_j^n, \nabla \mathbf{v}_\mathbf{n}^\mathbf{n}). \tag{6.11}$$

For the nonseparable model, we have an extra diffusive term $\frac{\Lambda_2}{\phi_n}\nabla \cdot (\phi_n \nabla \tau)$ in the right hand side of (6.9) and write it as $F(\tau, \nabla \mathbf{v}_n, \phi_n)$. Using boundary condition (6.5), we solve τ_j^n, $0 \le j \le M$, by (6.11) with $F(\tau_j^n, \nabla \mathbf{v}_n^n)$ replaced by $F(\tau_j^n, \nabla \mathbf{v}_n^n, \phi_n^n)$. The derivatives are discretized again by central differences. The overall scheme is second order in space and time.

7 Model Comparison in 1-D Transient Flows

Separable model 2 in the viscous limit ($\lambda_1 \to 0$) has been studied in [38, 39, 7] in both 1 and 2 space dimension. Here we revisit the nonlinear transient growth of the biofilm in 1-D using all three viscoelastic models with an emphasis on the comparison of the model predictions under shear. We limit our studies to the growth and expansion of biofilms that are homogeneous in the (x, z) plane alone using the numerical scheme alluded to in the previous section. Table 1 lists the ranges and values of the dimensional parameters used in our numerical investigations which are summarized from the currently available literature [23, 9, 21]. In the numerical study, the initial profile for ϕ_n is chosen as a step function (mimicking a localized distribution of the biofilm across the shear cell with a sharp interface between the biofilm and the solvent), the initial stress is assumed zero, and the nutrient concentration is initially saturated at the feeding level. We consider a constant shear velocity $\mathbf{v}_x = v_{shear} = 1$ imposed at $y = 1$ and the nutrient concentration c^* holds at a constant value at $y = 1$. The initial velocity profile is a nonlinear smooth interpolation between the shearing speed and the zero velocity at the lower boundary $y = 0$.

The measured biofilm relaxation time and viscosity vary with respect to the wall stress exerted on the rheometric device used in the measurement [37, 23]. The relaxation time can vary from 4.57 s to 169.5 s, an order of 37 folds difference between the high and the low value in one study [37, 23]. Most theoretical and computational studies on biofilms have been focused on the biofilm growth dynamics which is dominated by the viscous effect in terms of biofilm hydrodynamics. Since the three kinetic models developed in this paper differ predominantly in the viscoelastic stress constitutive equation, we conduct our comparative studies on model predictions focusing on the viscoelastic response. We use two relaxation time values in which the larger one is 55 folds of the smaller one.

Table 1: Parameter Values Used In Simulations

Symbol	Parameter	value	Unit
T	Temperature	303	Kelvin
γ_1	Distortional energy	1×10^{7}	m kg s^{-2}
γ_2	Mixing free energy	1×10^{17}	m^{-1} kg s^{-2}
χ	Flory-Huggins parameter	0.55 and 0.65	
λ	Mobility parameter	$1\times10^{-10}\sim1\times10^{-8}$	$kg^{-1}m^3s$
N	Generalized polymerization parameter	1×10^{3}	
μ	Max. Production rate	1.4×10^{-3}	$kgm^{-3}s^{-1}$
K_c	Half saturation constant for polymer growth	1×10^{-4}	kgm^{-3}
K_0	Half saturation constant for nutrient decay	5×10^{-4}	kgm^{-3}
A	Max. Consumption rate	0.1	$kgm^{-3}s^{-1}$
D_s	Substrate diffusion coefficient	2.3×10^{-9}	m^2s^{-1}
η_n	Viscosity of the EPS network	0.02	$kgm^{-1}s^{-1}$
η_{ps}	Viscosity of the bacteria in the polymer network	4.3×10^{2}	$kgm^{-1}s^{-1}$
η_s	Viscosity of solvent	1.002×10^{-3}	$kgm^{-1}s^{-1}$
ρ_n	Network density	1×10^{3}	kgm^{-3}
ρ_s	Network solvent	1×10^{3}	kgm^{-3}
c_0	Characteristic substrate concentration	1×10^{-3}	kgm^{-3}
h	Characteristic length scale	2×10^{-4}	m
t_0	Characteristic time scale	40	s
λ_1	Relaxation time	$50\sim2\times10^{3}$	s
a	Slip parameter (a)	0.92	
M	Number of spacial sub-intervals	$64\sim256$	

7.1 Highly elastic regime: $\Lambda_1 >> 1$

We first examine the models in the "highly elastic" regime: $\Lambda_1 = 2.5\times10^{3} >> 1$ and $\frac{1}{Re_n\Lambda_1}\sim O(1)$. Figure 1 depicts the profile of the solutions of the three models at $t = 200$ and the mobility parameter $\Lambda = 2.5\times10^{-7}$. We observe that the biomass grows due to the bacterium and EPS production capability and expands to the solvent region by the excessive flux resulted from solvent-polymer mixing dynamics. The step profiles in Figure 1(a) are ϕ_n at $t = 0$, and the smooth curves are ϕ_n at $t = 200$. The biomass growth is fueled by the availability of the nutrient so that the growth slows down when the nutrient concentration is low and eventually stops when it is depleted. We notice that the time scales in both growth and expansion are comparable at this mobility value so that the biomass in the biofilm region can be transported swiftly into the solvent region to fuel the expansion. Hence, we don't see the accumulation of biomass at the interface leading to anomalous growth there. The maintenance of sustainable level of nutrient at the interfacial region is achieved by its proximity to the nutrient rich solvent region as well as nutrient diffusion. The differences among results from the three models are essentially indistinguishable in this comparison. This is expected for separable model 2 and the nonseparable model (labeled as model 2 and 3 in the figures) since they have the same transport equation for ϕ_n and c. For separable model (labeled as model 1 in the figures), since the dimensionless mobility parameter Λ is at most 2.5×10^{-7} and very small, the contribution from the extra term $\frac{1}{2}\Lambda\phi_n\nabla(\mathrm{tr}(\tau)-\frac{\Gamma_2}{N}\ln\det(\tau+\frac{\Gamma_2}{N}\mathbf{I}))$ in the excessive flux is also very small. Thus the ϕ_n plotted in Figure 1(a) shows no visible difference. A more detailed comparison is given in Figure 2 which depicts the difference between ϕ_n computed by model 1 and 2 (left picture) and by model 2 and 3 (right picture) at $t = 200$, respectively. We observe that model 2 and 3 give virtually identical result of ϕ_n, which differs

from the result of model 1 by an order of 10^{-5}. Therefore, the coupling between ϕ_n and stress tensor τ in model 1 does make a difference. However, in the current parameter value range, the difference is so small and essentially indistinguishable.

To reveal more details about the nonlinear expansion and growth of biomass and dynamics of other components in the mixture, we plot the profile of the nutrient concentration c at $t = 200$ in the figure as well. The initial distribution of the nutrient is assumed uniform matching the boundary condition at the feeding end. We observe that the nutrient concentration c depletes more quickly deep in the region occupied by the bulk biomass than near the biofilm-solvent interface.

The expansion direction of the biomass is perhaps best monitored by its velocity. The figure depicts the nonzero polymeric velocity component $v_{ny} = v_y^e$ in the y-direction and the polymeric velocity $v_{nx} = v_x$ in the x-direction. The velocity components in both directions are fairly small in magnitudes. Given the large bacterial viscosity in the effective polymer, the motion of the biomass in the biofilm region is very slow compared to that of the solvent. The growth of the biofilm in the y-direction is signatured by the largely positive polymeric velocity component v_y^e although it experiences a negative local minimum at the interface at $t = 200$. The negative transient velocity indicates a transient decay in the biofilm at $t = 200$. In general, an overwhelmingly positive v_y^e causes the slow growth of the biofilm's thickness. The equation for $\mathbf{v}_x$ is essentially a diffusion equation with the Dirichlet boundary condition at $y = 0$ and $y = 1$. Hence, we see an approximately linear profile in v_x in the regions occupied by the biofilm and the solvent, respectively.

Since the EPS in the biomass is modeled as a polymer network consisting of elastic dumbbell strands, the elastic stress dynamics is worthy of a detailed interrogation to explore the mechanical stress exerted on the EPS polymer network. Figure 1(e,f) depict the shear ($\phi_n\tau_{xy}$) and the normal elastic stress component ($\phi_n\tau_{yy}$) at $t = 200$, respectively. Both stresses peak behind the interface between the biofilm and the pure solvent in the biofilm region. The peak of the shear and normal stress correlates well with the peak of the velocity component v_y in which there exists a local maximum at the interface. The results obtained from all models are identical numerically.

At a smaller mobility, the transient biofilm profile and other hydrodynamic variables agree even better among the predictions by the three models in the parameter regime investigated. Figure 3 depicts the solutions for all three models at $t = 200$ and $\Lambda = 2.5 \times 10^{-9}$. The biomass volume fraction profile exhibits some active growth and accumulation of biomass at the interface at the smaller mobility value. This active growth takes a toll on the nutrient concentration at the interface as well, where the nutrient concentration exhibits a local minimum corresponding to the local maximum in the biomass fraction. This is the consequence of the fact that the growth time scale exceeds that of the transport time scale at this mobility parameter leading to a local accumulation of the biomass and thereby the noticeable consumption of the nutrient. The elastic shear stress value is considerably small in the biofilm than in the previous case. The fluctuation at the interface in the elastic shear stress is not seen at $t = 200$. Figure 4 exploits the fine details of the velocity inside the biofilm region during the shearing process at $t = 200$ and $\Lambda = 2.5 \times 10^{-9}$. It reveals the magnitude of the slow motion of the biofilm in the x-direction leading up to the edge of the interface.

We also examine the solution of the system at a different mixing parameter $\chi = 0.65$ when there is a growth mode due to the polymer-solvent mixing dynamics. Figure 5 depicts the solution at $t = 200$ and $\Lambda = 2.5 \times 10^{-9}$. When the growth mode due to the mixing dynamics exists, the biomass growth dominates. At $t = 200$, there is little expansion of the biofilm into the pure solvent region shown. To the contrary, the active growth of the biomass tends to pull the biomass into the the active growth region around the interface in the cell. This is best shown in the velocity v_y where it is negative at the interface. This is related to the nucleation process inherent to the Cahn-Hilliard dynamics in this parameter regime. Meanwhile, the elastic shear and the normal stress component all peak at the fastest growing spot. The situation is alleviated as the mobility parameter or the shear speed increases. Once again, the three models give virtually identical predictions.

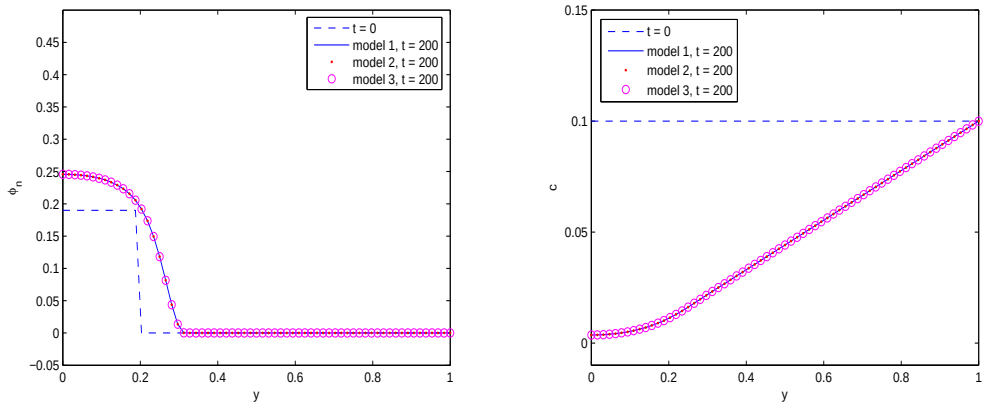

(a) ϕ_n

(b) c

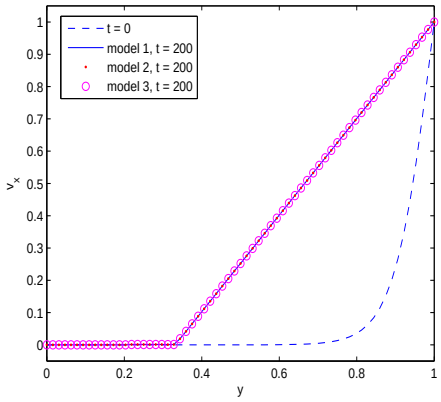

(c) v_x

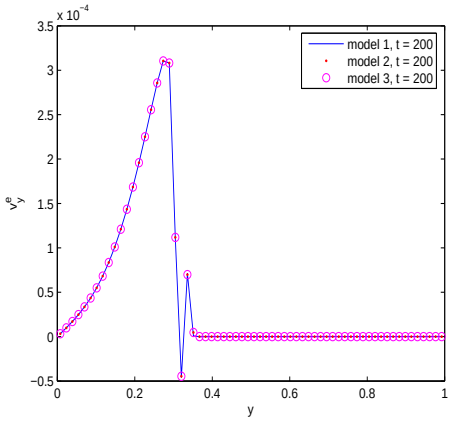

(d) v_y^e

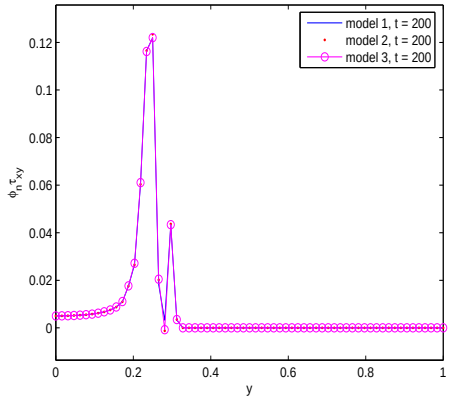

(e) $\phi_n \tau_{xy}$

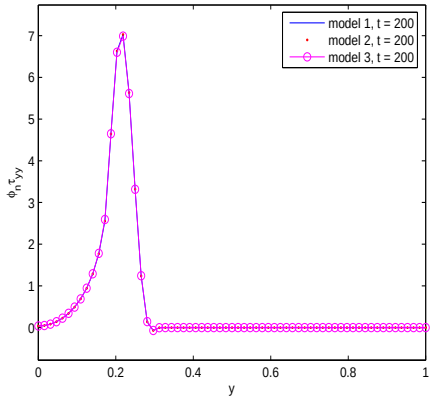

(f) $\phi_n \tau_{yy}$

Figure 1: Solutions of the three models at $t = 200$, mobility parameter $\Lambda = 2.5 \times 10^{-7}$, mixing parameter $\chi = 0.55$, and relaxation time $\Lambda_1 = 2.5 \times 10^3$. The separable model 1 and 2 are referred to as model 1 and 2 while the nonseparable model is referred to as model 3 in the text and the figures. (a). The biomass volume fraction ϕ_n; (b). the nutrient concentration c; (c). the velocity component in the x-direction v_x; (d). the velocity component in the y-direction $v_y = v_y^e$; (e). the elastic shear stress $\phi_n \tau_{xy}$; (f). the elastic normal stress $\phi_n \tau_{yy}$. The three models' predictions are essentially indistinguishable in this parameter regime.

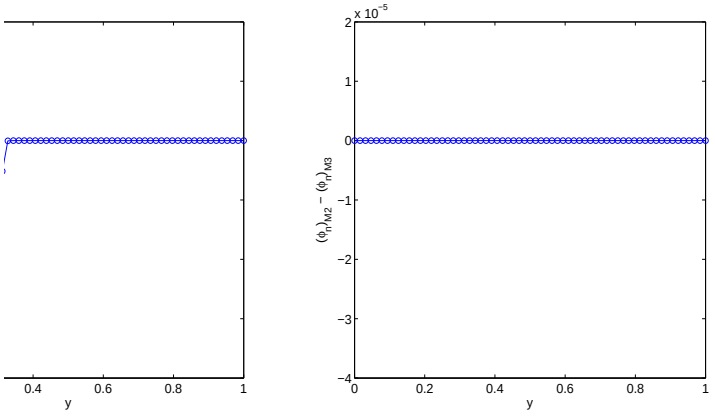

Figure 2: Difference of the biomass volume fraction between model 1 and 2 as well as model 2 and 3 at $t = 200$. (a). The difference in the biomass volume fraction between model 1 and model 2. The largest difference is in the order of $O(10^{-5})$. (b). The difference in the biomass volume fraction between model 2 and model 3. Model 2 and 3 give virtually identical results. Parameter values are identical to the ones used in Figure 1.

7.2 Viscoelastic regime

We next consider the regime where Λ_1 decreases to 50 at fixed $\Lambda = 2.5 \times 10^{-7}$. The velocity component v_y starts to show deviations between the one calculated from model 1 and those by model 2 and 3 at $t = 60$ shown in Figure 6. v_y predicted by separable model 2 and the nonseparable model tends to show tamed fluctuations at the interface than that of separable model 1. The shear stress profile predicted by three models show some differences as well, in that separable model 2 and the nonseparable model give qualitatively the same predictions while separable model 1 yields a fluctuating elastic shear stress near the interface. The normal stress prediction by the three models in $\phi_n \tau_{yy}$ are all comparable however. Figure 7 depicts the difference between ϕ_n computed using model 1 and 2 (left picture) and using model 2 and 3 (right picture) at $t = 60$, respectively. We again observe that model 2 and 3 give virtually identical result for ϕ_n, which differs from the result of model 1 in the order of 10^{-3}. Although the difference in ϕ_n is still invisible from Figure 6(a), it is two orders of magnitude larger than the difference shown in Figure 2. *The apparent fluctuations in velocity component v_y and thereby the elastic shear stress $\phi_n \tau_{xy}$ from model 1 are attributed to the larger deviation in ϕ_n from model 1 in the current parameter value range.* We remark that the results shown in the figure are computed using mesh size $\Delta y = 1/64$, and computations with mesh size $\Delta y = 1/128, 1/256, 1/512$ give the same result which indicates that the stress fluctuation is space is not an artifact of the coarse mesh, rather it's the constitutive response to the slight variation in the biomass volume fraction and the associated excessive velocity variation. Furthermore, since the governing equations for the stress τ are the same for separable model 1 and 2, and are solved by the same numerical scheme, the difference in τ should be attributed to the difference between these two models. Namely, ϕ_n and τ are coupled in separable model 1 but not in separable model 2. We examine the difference between separable model 2 and the nonseparable model further along in the simulation. At $t = 200$, the difference in the elastic stress starts to emerge as shown in Figure 8. The solutions are comparable to those depicted in Figure 1 except that the two elastic stress components predicted using separable model 2 differ from those predicted by the nonseparable model in the interfacial region. The difference is quantitative though.

At mixing parameter $\chi = 0.65$, the biofilm dynamics in the viscoelastic limit is analogous to the highly elastic limit; the growth instability due to the biomass-solvent mixing along with the biomass production dominates leading to biomass growth in volume fraction in the originally occupied location in biofilm. There

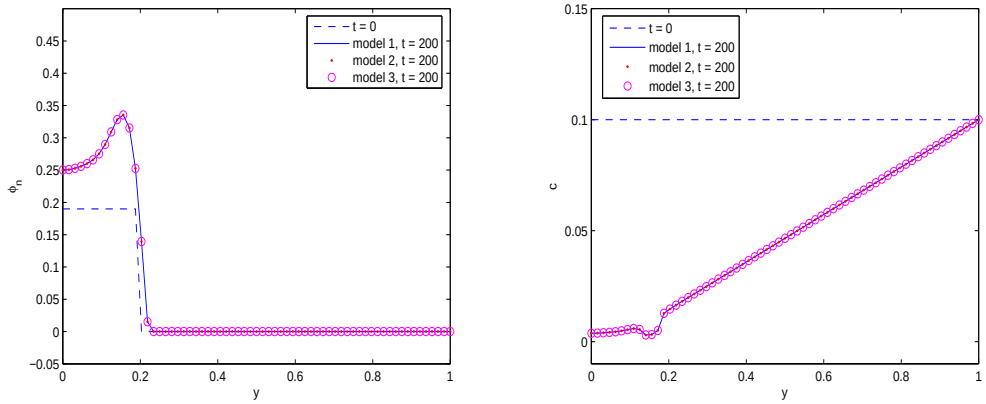

(a) ϕ_n

(b) c

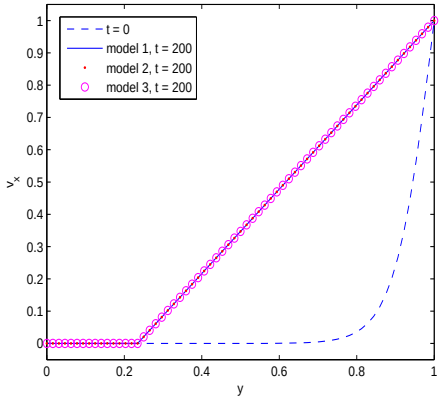

(c) v_x

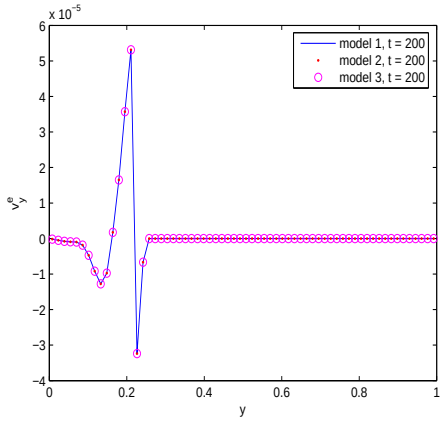

(d) v_y^e

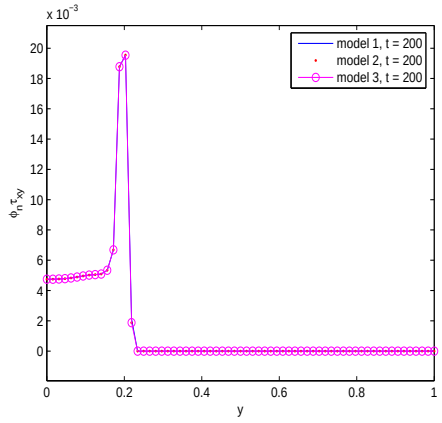

(e) $\phi_n \tau_{xy}$

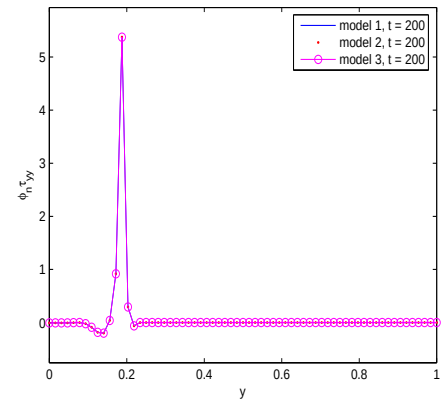

(f) $\phi_n \tau_{yy}$

Figure 3: Solutions of the three models at $t = 200$, mobility parameters $\Lambda = 2.5 \times 10^{-9}$, mixing parameter $\chi = 0.55$, and relaxation time $\Lambda_1 = 2.5 \times 10^3$. The nutrient is consumed the most at the front of the biofilm. The three models' predictions are essentially indistinguishable.

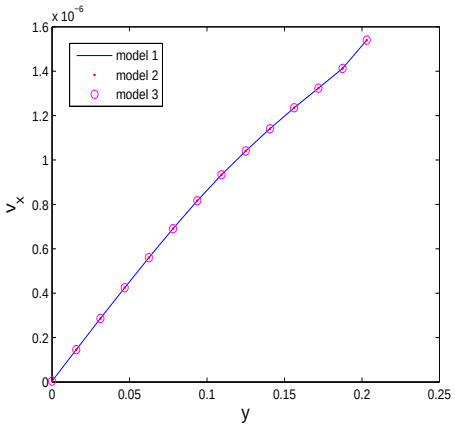

Figure 4: Blow-up of v_x in the biofilm region with respect to solutions of all three models at $t = 200$. The results are essentially indistinguishable.

is a slight pulling back at the biofilm-solvent interface due to biomass nucleation. The growth velocity is an order of magnitude weaker than in the highly elastic limit. Figure 9 plots a solution at $t = 200$ and $\chi = 0.65$.

Finally, we comment on the solutions at a smaller mobility in the viscoelastic limit. The general trend of the solution follows that alluded to in the highly elastic limit for ϕ_n. The solutions predicted by the three models agree very well. The elastic shear stress are all positive with the largest value given by separable model 1.

In summary, the three models give qualitatively the same results in the parameter range we investigated. When mobility is low, the growth mode dominates. Otherwise, the spatial expansion of the biofilm and local growth occur simultaneously. Minor differences are identified among separable model 1, separable model 2 and the nonseparable model. The volume fraction transport equation in separable model 1 couples to the stress constitutive equation, Whereas, that of the separable model 2's equation for ϕ_n decouples from the elastic stress equation and is driven by the equation of c, so does the nonseparable model. But, the nonseparable model has a diffusive stress constitutive equation which couples to the equation of ϕ_n and requires a no-flux boundary condition for the stress tensor at the boundary. Ideally the nonseparable model is the model we should use since it does not impose any a priori assumption on the distribution of the EPS polymer network (i.e., the separability of the pdf distribution). However, this comparative study has demonstrated the competency of separable model 2 in the parameter regime we investigated, which is simpler than the nonseparable model.

8 Conclusions

We have systematically developed a set of kinetic theories for the biofilm, a mixture of biomass and solvent, using the one-fluid multi-component formulation to model the nonlinear growth and transport of the biomass (extracellular polymeric substances EPS and bacteria) and the interaction between the biomass and nutrient and solvent in flows. The theoretical framework allows detailed conformational information of the EPS polymer network strand to be accounted for and has the potential to be expanded to incorporate more microscopic details about the biomass and cell-to-cell communication like quorum sensing in the future. Adopting three distinctive formulations of the dominating mean field force or velocity in the translational diffusion in the Smoluchowski equation for a normalized distribution ψ (a statistical weight,) we derive three distinct models for the biomass-solvent mixture. All these models are valid not only within the biofilm region

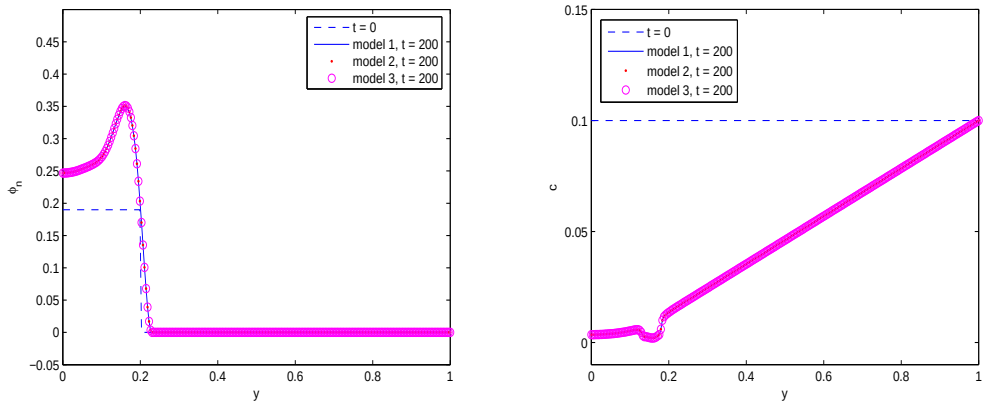

(a) ϕ_n

(b) c

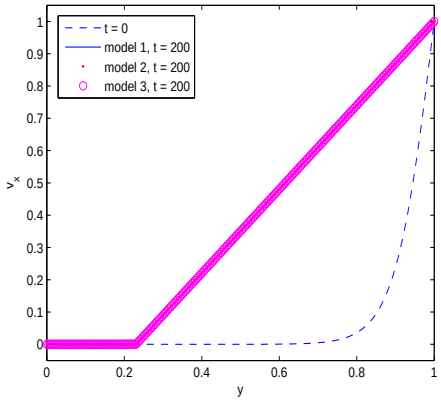

(c) v_x

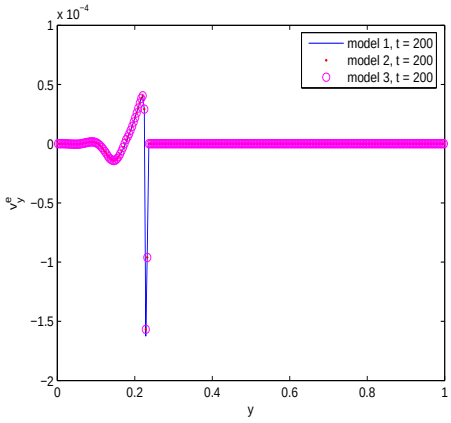

(d) v_y^e

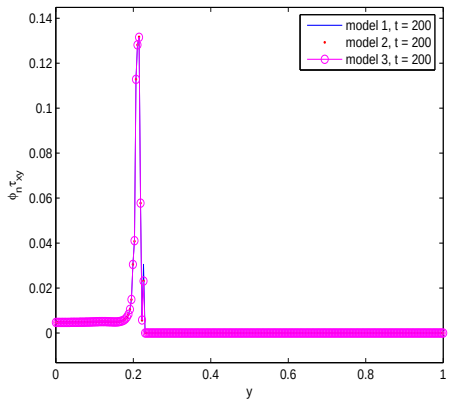

(e) $\phi_n \tau_{xy}$

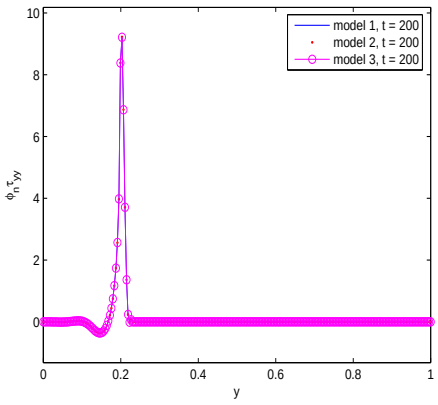

(f) $\phi_n \tau_{yy}$

Figure 5: Solutions of the three models at $t = 200$, mobility parameter $\Lambda = 2.5 \times 10^{-9}$, mixing parameter $\chi = 0.65$, and relaxation time $\Lambda_1 = 2.5 \times 10^3$. The results are essentially indistinguishable.

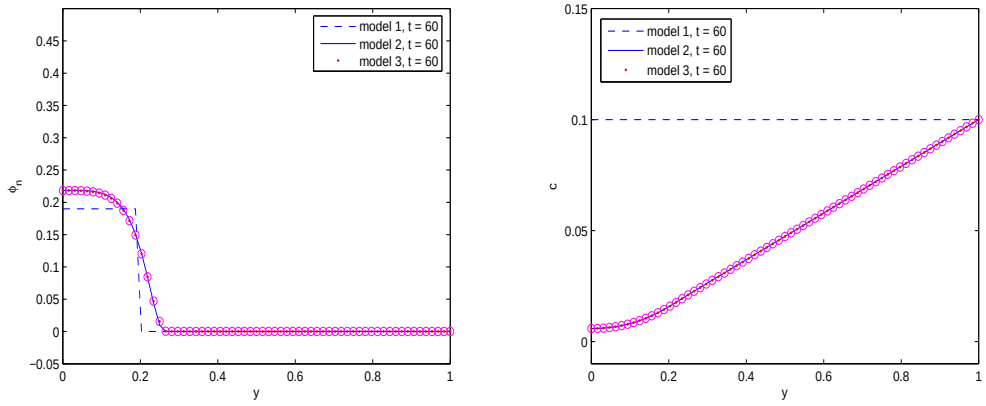

(a) ϕ_n

(b) c

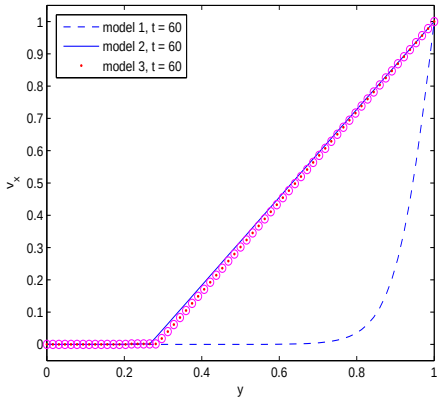

(c) v_x

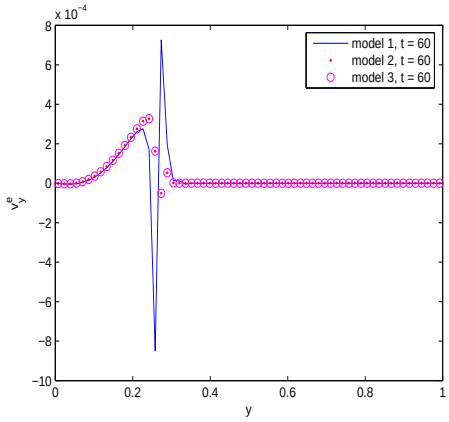

(d) v_y^e

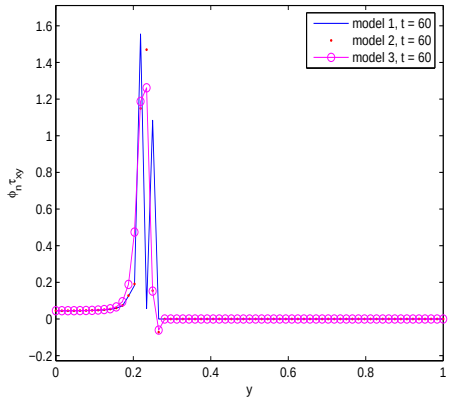

(e) $\phi_n \tau_{xy}$

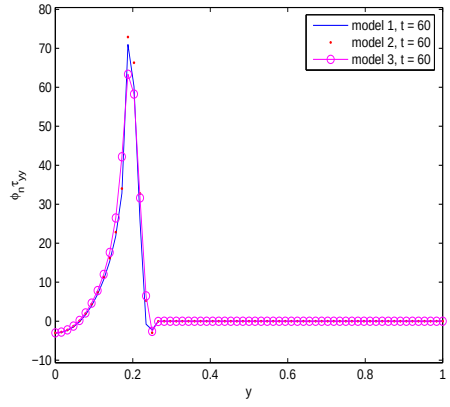

(f) $\phi_n \tau_{yy}$

Figure 6: Solutions of all three models at $t = 60$, mobility parameter $\Lambda = 2.5 \times 10^{-7}$, mixing parameter $\chi = 0.55$, and relaxation time $\Lambda_1 = 50$. Model 1 exhibits the largest fluctuation in velocity and elastic stress at the biofilm-solvent interface while the other two models show mild fluctuations.

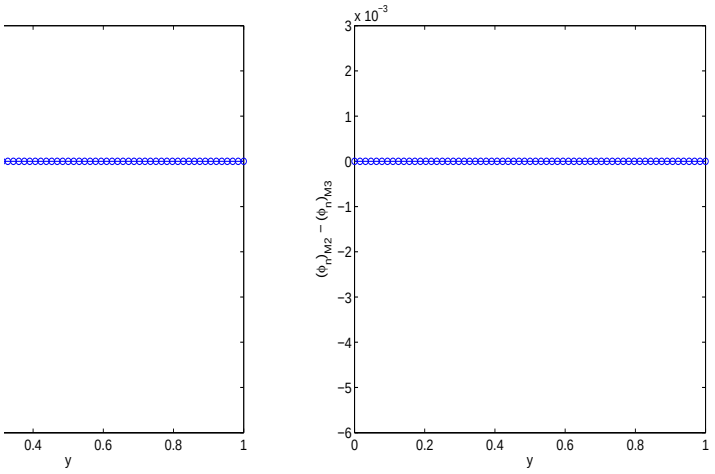

Figure 7: Biomass volume fraction difference between two pairs of models at $t = 60$. (a). The difference between model 1 and model 2 at $t = 60$. The largest difference is in the order of $O(10^{-3})$. (b). The difference between model 2 and model 3 at $t = 60$. The two models give virtually identical results. Parameter values are identical to those used in Figure 6.

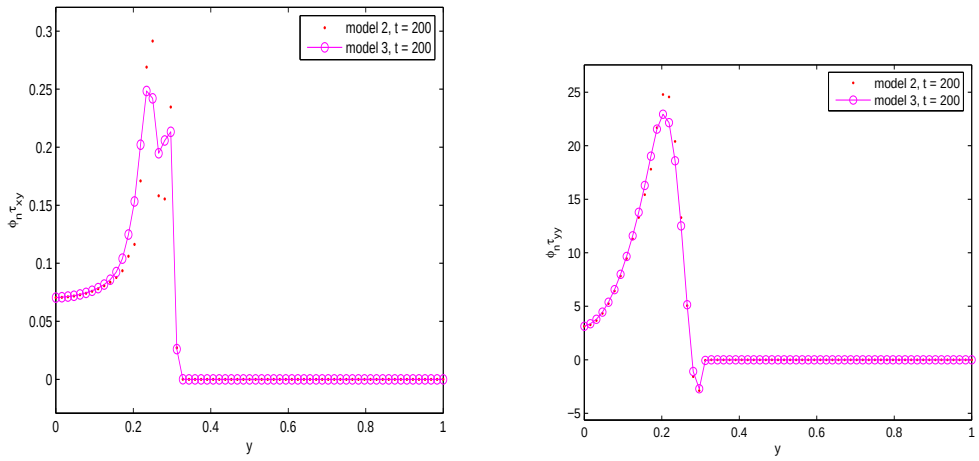

(a) $\phi_n \tau_{xy}$ (b) $\phi_n \tau_{yy}$

Figure 8: Solutions of model 2 and 3 at $t = 200$, mobility parameter $\Lambda = 2.5 \times 10^{-7}$, mixing parameter $\chi = 0.55$, and relaxation time $\Lambda_1 = 50$. The fluctuation in stress is amplified in long time demonstrating that model 3 exhibits the smallest fluctuation among the three models investigated.

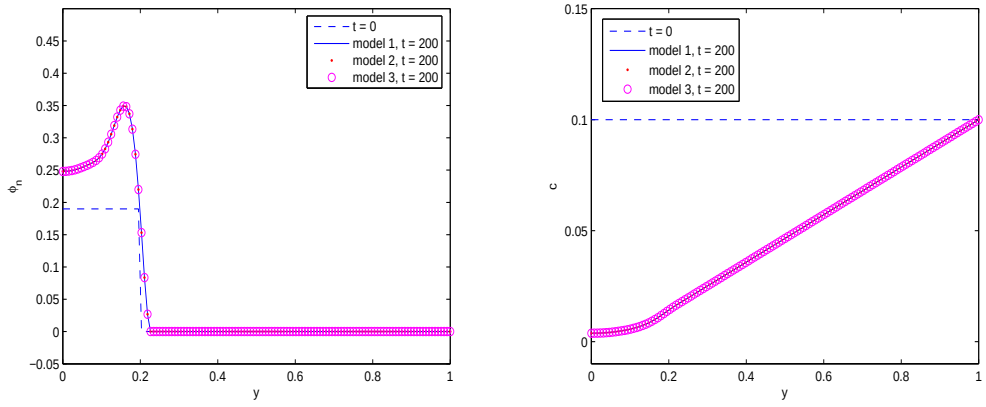

(a) ϕ_n

(b) c

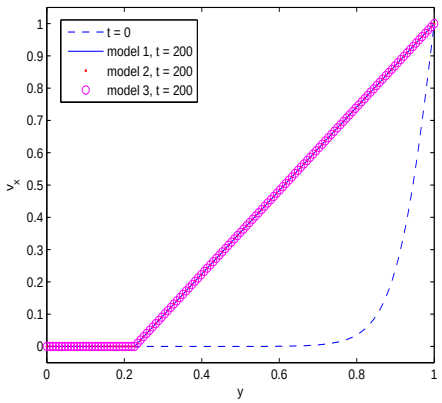

(c) v_x

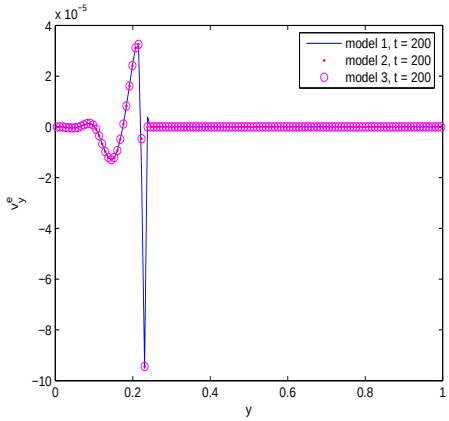

(d) v_y^e

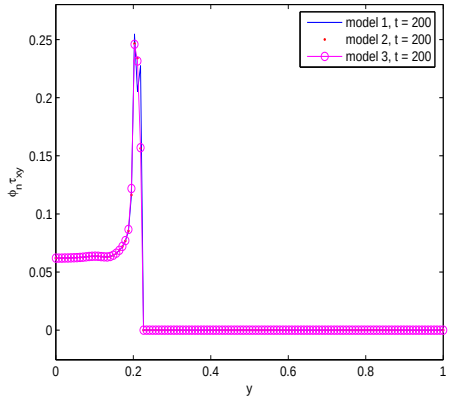

(e) $\phi_n \tau_{xy}$

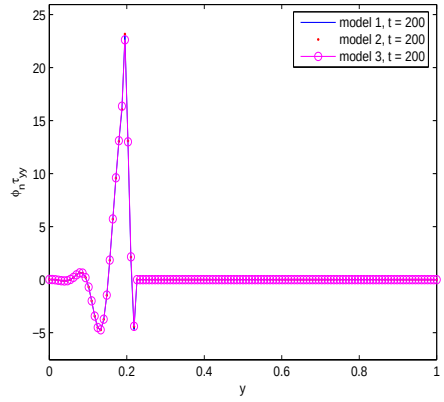

(f) $\phi_n \tau_{yy}$

Figure 9: Solutions of the three models at $t = 200$ and mobility parameter $\Lambda = 2.5 \times 10^{-9}$, mixing parameter $\chi = 0.65$, and relaxation time $\Lambda_1 = 50$. The results from model 2 and 3 are essentially indistinguishable. The stress fluctuation from model 1 differs slightly from those from model 2 and model 3.

but also in the pure solvent region making them bona fide multiphase hydrodynamic models. A specific contact is made between separable model 2 and the continuum phase field model developed previously based on a phenomenological approach establishing the microscopic foundation for the phase field model, which has been used to study biofilm dynamics in 3-D flow chambers [38, 7]. We then analyze the linear stability properties of a set of constant steady states shared by all three models revealing the potential long-wave instability in the models for the biofilm growth in addition to the inherent biomass growth mechanism for all waves. Finally, we compare the three models on their transient nonlinear dynamics in 1-D shear flows in the viscoelastic regime with only one relaxation time. Our numerical results show that all three models predict qualitatively the same behavior with the diffusive stress model rendering a smoother stress profiles and reduced stress values in the parameter range investigated. For model 1, the biomass profile and the associated excessive velocity for the biomass leads to a elastic stress fluctuation within the biomass-solvent interface. This feature is robust in model 1 and is believed to be the result of enhanced coupling between the stress and the biomass transport that is unique in this model. In the viscous limit, the three models collapse into a single multiphase phase field model which was studied extensively in [38, 39, 7]. Extension of this formulation can be made to deal with multiple species of biomass and thereby allow a full coupling of quorum sensing mechanism. This work will be forthcoming in a sequel.

Acknowledgment and Disclaimer

Effort sponsored by the Air Force Office of Scientific Research, Air Force Materials Command, USAF, under grant number FA9550-08-1-0107 and the National Science Foundation through grants DMS-0605029, DMS-0626180, DMS-0819051, DMS-0908330 are gratefully acknowledged.

References

[1] E. Alpkvist and I. Klapper, A Multidimensional Multispecies Continuum Model for Heterogeneous Biofilm Development, Bull. Math. Biol., 69 (2007), 765-789.

[2] A. N. Beris and B. Edwards, *Thermodynamics of Flowing Systems*, Oxford Science Publications, New York, 1994.

[3] R. B. Bird, R. C. Armstrong, O. Hassager, *Dynamics of Polymeric Liquids*, vol. 1 & 2, John Wiley and Sons, New York, 1987.

[4] J. W. Cahn and J. E. Hilliard, Free energy of a nonuniform system. I: interfacial free energy, J. Chem. Phys., 28 (1958), 258-267.

[5] J. W. Cahn and J. E. Hilliard, Free energy of a nonuniform system-III: Nucleation in a 2-component incompressible fluid, J. Chem. Phys., 31 (3) (1959), 688-699.

[6] P. M. Chaikin and T.C. Lubensky, *Principles of Condensed Matter Physics*, Cambridge University Press, Cambridge, 1995.

[7] Chen Chen, Mingming Ren, Ashok Srinivasan and Qi Wang, 3-D simulations of biofilm-solvent interaction, East Asian Journal on Applied Mathematics, 1 (2011), 197-214.

[8] N. G. Cogan and J. Keener, Channel Formation in Gels, Siam J. Applied Math., 65 (6) (2005), 1839-1854.

[9] N. Cogan and J Keener, The Role of Biofilm Matrix in Structural Development, Mathematical Medicine and Biology, 21(2) (2004),147-166.

[10] J.W. Costerton, Z. Lewandowski, D.E. Caldwell, D.R. Korber and H.M. Lappin-Scott, Microbial biofilms, Annu Rev Microbiol 49 (1995), 711-745.

[11] B. Costerton, Medical Biofilm Microbiology: The Role of Microbial Biofilms in Disease, Chronic Infections, and Medical Device Failure, CD-ROM, Montana State University, 2003.

[12] M. E. Davey and G. A. O'toole, Microbial Biofilms: from Ecology to Molecular Genetics Microbiology and Molecular Biology Reviews, 64 (4) (2000), 847-867.

[13] E. De Lancey Pulcini, Bacterial biofilms: a review of current research,Nephrologie, 22(8) (2001), 439-441 .

[14] J. Dockery and I.Klapper, Finger formation in biofilm layers, SIAM J. Appl. Math., 62 (2002), 853-869 .

[15] M. Doi and S. F. Edwards, *The Theory of Polymer Dynamics*, Oxford Science Publications, Oxford, 1986.

[16] M. Doi, *Introduction to Polymer Physics*, Oxford Science Publications, Oxford, 1995.

[17] P. J. Flory, *Principles of Polymer Chemistry*, Cornell University Press, Ithaca, NY, 1953.

[18] D. J. Hassett, P. A. Limbach, R. F. Hennigan, K. E. Klose, R. E. Hancock, M. D. Platt, D. F. Hunt, Bacterial biofilms of importance to medicine and bioterrorism: proteomic techniques to identify novel vaccine components and drug targets, Expert Opin Biol Ther, 3(8) (2003),1201-1207.

[19] R. G. Larson, *The Rheology of Complex Fluids*. Oxford University Press, New York, 1998.

[20] C. A. A. Lima, R. Ribeiro, E. Foresti and M. Zaiat, Morphological Study of Biomass During the Start-Up Period of a Fixed-Bed Anaerobic Reactor Treating Domestic Sewage, Brazilian Archives of Biology and Technology.

[21] N. Cogan and J Keener, Channel formation in gels, SIAM J. Appl. Math., 65 (2005), 1839-1854.

[22] I. Klapper, Effect of Heterogeneous Structure in Mechanically Unstressed Biofilms on Overall Growth, Bulletin of Mathemstical Biology, 66 (2004), 809-824.

[23] I Klapper, C. J. Rupp, R. Cargo, B. Purvedorj, P. Stoodley, Viscoelastic Fluid Description of Bacterial Biofilm Material Properties, Biotechnology and Bioengineering, 80(3) (2002), 289-296.

[24] I. Klapper and J. Dockery, Role of Cohesion in the Material Description of Biofilms, Phys. Rev. E 74, (2006), 031902.

[25] C. S. Laspidou and B. E. Rittmann, Modeling biofilm complexity by including active and inert biomass and extracelluar polymeric substances, Biofilm, 1 (2004), 285-291.

[26] J. Lowengrub and L. Truskinovsky, Quasi-incompressible Cahn-Hilliard fluids and topological transitions. R. Soc. Lond. Proc. Ser. A Math. Phys. Eng. Sci. 454 (1978) (1998), 2617-2654.

[27] S. T. Milner, Dynamical Theory of Concentration Fluctuations in Polymer Solutions under Shear, Phys. Rev. E, 48(5) 1993, 3674-3691.

[28] G. O'Toole, H. B. Kaplan, R. Kolter, Biofilm Formation as Microbial Development, Annual Review of Microbiology, 54 (2000), 49-79.

[29] C. Picioreanu, M. van Loosdrecht, J. Heijnen, Mathematical modeling of biofilm structure with a hybrid differential-discrete cellular automaton approach. Biotech. Bioeng., 58 (1998), 101-116.

[30] C. Picioreanu, M. van Loosdrecht, J. Heijnen, Multidimensional modelling of biofilm structure, Biotech. Microbial Biosystems: New Frontiers, Proceedings of the 8th International Symposium on Microbial Ecology, Bell CR, Brylinsky M, Johnson-Green P (eds), Atlantic Canada Society for Microbial Ecology, Halifax, Canada, 1999.

[31] C. Picioreanu, M. J-U Kreft, M. van Loosdrecht, Particle-based multidimensional ultispecies biofilm models, Applied and Envrionmental Microbiology, May (2004), 3024-3040.

[32] C. Picioreanu, J. B. Xavier, M. van Loosdrecht, Advances in mathematical modeling of biofilm structure, Biofilm, 1 (2004), 337-349.

[33] H. Tanaka, Viscoelastic Model of Phase Separation, Phys. Rev. E, 56(4) (1997), 4451-4462.

[34] C. Wolgemuth, E. Hoiczyk, D. Kaiser, and G. Oster, How Myxobacteria Glide, Current Biology, 12 (2002), 369-377.

[35] Pengtao Yue, James J. Feng, Chun Liu, and Jie Shen, A Diffuse-Interface Method for Simulating Two-Phase Flows of Complex Fluids. J. Fluid Mech. 515 (2004), 293-317.

[36] Pengtao Yue, James J. Feng, Chun Liu, Jie Shen, Viscoelastic effects on drop deformation in steady shear. J. Fluid Mech., 540 (2005), 427-437.

[37] P. Stoodley,Z. Lewandowski, J. D. Boyle, and H. M. Lappin-Scott, The formation of migratory ripples in a mixed species bacterial biofilm growing in turbulent flows. Environ Microbiol, 1 (1999), 447-457.

[38] T. Zhang, N. Cogan, and Q. Wang, Phase-Field Models for Biofilms. I. Theory and 1-D Simulations, Siam J. Appl. Math., 69 (3) (2008), 641-669.

[39] T. Zhang, N. Cogan, and Q. Wang, Phase-Field Models for Biofilms. II. 2-D Numerical Simulations of Biofilm-Flow Interaction, Communications in Computational Physics, 4 (2008), 72-101.